

POLITECNICO DI TORINO

Corso di Laurea Magistrale in Ingegneria Meccanica

Mechanical Engineering: Mechanical Design



Master's Degree Thesis

Multi-objective Optimization for Aeronautical Gears

Supervisors:

Prof. Daniele Botto

Ing. Luca Ronchiato

Candidate:

Serena Occhipinti

July 2020

Contents

<i>Sommario</i>	<i>VII</i>
<i>Abstract</i>	<i>IX</i>
<i>Acknowledgments</i>	<i>XI</i>
<i>Introduction</i>	<i>2</i>
1. <i>Literature</i>	<i>5</i>
1.1 <i>Spur Gears</i>	<i>5</i>
1.2 <i>Helical Gears</i>	<i>6</i>
1.3 <i>Bevel Gears</i>	<i>7</i>
1.4 <i>Worm Gears</i>	<i>7</i>
2. <i>State of art</i>	<i>9</i>
2.1 <i>Micro-geometrical optimization methods</i>	<i>9</i>
2.1.1 <i>A method to define profile modification of Spur Gear</i>	<i>10</i>
2.1.2 <i>Optimization methods for spur gear dynamics</i>	<i>2</i>
2.2 <i>Geometrical optimization methods</i>	<i>3</i>
2.2.1 <i>Multi-objective Dynamics Optimization for Aeronautical Gears</i>	<i>3</i>
2.2.2 <i>Static and Dynamic Topology Optimization</i>	<i>4</i>
3. <i>Tool structure</i>	<i>5</i>
3.1 <i>User Inputs</i>	<i>5</i>
3.2 <i>Toll outputs</i>	<i>7</i>
3.2.1 <i>Pareto Front</i>	<i>8</i>
3.3 <i>Design space definition</i>	<i>9</i>
3.4 <i>Mesh generation</i>	<i>10</i>
3.5 <i>Time Response Analysis</i>	<i>13</i>
3.5.1 <i>Nyquist Theorem</i>	<i>14</i>
3.6 <i>Campbell diagram</i>	<i>15</i>
3.7 <i>Optimization process</i>	<i>17</i>
3.7.1 <i>Latin Optimal Hypercube Sampling</i>	<i>17</i>
3.7.2 <i>Gradient Descent Method</i>	<i>18</i>
4. <i>Objective functions</i>	<i>21</i>
4.1 <i>Mass Function</i>	<i>21</i>
4.1.1 <i>Pappus-Guldin Second Theorem</i>	<i>21</i>

4.2	<i>Risk-Factor function</i>	22
5.	<i>Two-Parameters Optimization</i>	26
5.1	<i>Results validation</i>	27
5.1.1	<i>CASE 1 - Ring</i>	27
5.1.2	<i>CASE 2 – Spur Gear</i>	29
6.	<i>Four-Parameters Optimization</i>	35
6.1	<i>Spur Gear</i>	36
6.1.1	<i>Optimal geometry</i>	37
6.1.2	<i>Geometry with minimal Risk-Factor</i>	40
7.	<i>Conclusions</i>	43
	<i>Appendix A</i>	45
	<i>FEM analysis</i>	45
	<i>Mesh</i>	46
	<i>Bibliography</i>	48

List of figures

<i>FIGURE 1: ACARE OBJECTIVES</i>	2
<i>FIGURE 2: SPUR GEARS</i>	5
<i>FIGURE 3: HELICAL GEARS</i>	6
<i>FIGURE 4: CROSSED HELICAL GEARS</i>	6
<i>FIGURE 5: STRAIGHT BEVEL GEARS - SPIRAL BEVEL GEARS - HYPOID BEVEL GEARS</i>	7
<i>FIGURE 6: WORM GEARS</i>	8
<i>FIGURE 7: PROFILE MODIFICATION PARAMETERS</i>	10
<i>FIGURE 8: PINION TIP RELIEF AND ROLL ANGLE</i>	10
<i>FIGURE 9: DEFINITION OF SAP AND EAP</i>	2
<i>FIGURE 10: DYNAMIC MODEL OF SPUR GEARS</i>	2
<i>FIGURE 11: BEZIER CURVES</i>	3
<i>FIGURE 12: TOPOLOGY OPTIMIZATION</i>	4
<i>FIGURE 13: REPRESENTATION OF THE TOOL STRUCTURE</i>	5
<i>FIGURE 14: EXAMPLE OF GEOMETRY INPUT DATA</i>	6
<i>FIGURE 15: EXAMPLE OF MODE PLOT</i>	7
<i>FIGURE 16: TIME RESPONSE AND CAMPBELL DIAGRAM</i>	7
<i>FIGURE 17: PARETO FRONT</i>	8
<i>FIGURE 18: REPRESENTATION OF PARETO FRONT</i>	9
<i>FIGURE 19: DESIGN AND NON-DESIGN SPACES</i>	10
<i>FIGURE 20: FIRST STEP OF MESH GENERATION</i>	10
<i>FIGURE 21: SERENDIPITY AXISYMMETRIC ELEMENT</i>	11
<i>FIGURE 22: 3D EXPANSION OF THE 2D MESH</i>	11
<i>FIGURE 23: MESH, CONSTRAINED AND TIME RESPONSE NODES</i>	12
<i>FIGURE 24: FLOW CHART OF THE SECOND BLACK-BOX CODE</i>	15
<i>FIGURE 25: REPRESENTATION OF EO EXCITATIONS ON CAMPBELL DIAGRAM</i>	16
<i>FIGURE 26: EXAMPLE OF INVESTIGATION OF POSSIBLE RESONANCE POINTS</i>	16
<i>FIGURE 27: EXAMPLE OF THREE LATIN 2D SAMPLING</i>	18
<i>FIGURE 28: INEFFECTIVE AND OPTIMAL LHS</i>	18
<i>FIGURE 29: FLOW CHART OF THE OPTIMIZATION PROCESS</i>	20
<i>FIGURE 30: SOLID OF REVOLUTION</i>	22
<i>FIGURE 31: RISK FUNCTION ENVELOPE</i>	24
<i>FIGURE 32: RISK-FACTOR FORMULATION</i>	25
<i>FIGURE 33: SIMPLIFIED GEOMETRY SECTION AND 3D EXPANSION</i>	26
<i>FIGURE 34: TWO-PARAMETERS OPTIMIZATION GEAR SECTION</i>	26
<i>FIGURE 35: REPRESENTATION OF FORCES AND CONSTRAINS OF TEST CASE 1</i>	27
<i>FIGURE 36: CASE1 – PLOT OF MASS, RISK-FACTOR AND OBJECTIVE FUNCTIONS</i>	28
<i>FIGURE 37: CASE 1 - PARETO FRONT</i>	29
<i>FIGURE 38: CASE2- FORCES AND CONSTRAINS</i>	30
<i>FIGURE 39: CASE 2- PLOT OF MASS, RISK-FACTOR AND OBJECTIVE FUNCTIONS</i>	30
<i>FIGURE 40: CASE 2- PLOTS OF THE TERMS OF THE RISK FACTOR FUNCTION</i>	31
<i>FIGURE 41: CASE 2 - OPTIMAL GEAR SECTION</i>	32

<i>FIGURE 42: CAMPBELL DIAGRAM AND TIME RESPONSE OF THE OPTIMAL GEAR SECTION</i>	32
<i>FIGURE 43: OPTIMAL SECTION - RISK FUNCTION ENVELOPE</i>	33
<i>FIGURE 44: PARETO FRONT</i>	34
<i>FIGURE 45: REPRESENTATION OF THE OPTIMIZATION PARAMETERS</i>	35
<i>FIGURE 46: PARETO FRONT OF SPUR GEAR OPTIMIZATION</i>	36
<i>FIGURE 47: OPTIMAL GEOMETRY</i>	37
<i>FIGURE 48: CAMPBELL DIAGRAM AND TIME RESPONSE OF THE OPTIMAL GEOMETRY</i>	38
<i>FIGURE 49: RISK-FUNCTION ENVELOPE OF THE OPTIMAL GEOMETRY</i>	38
<i>FIGURE 50: GEOMETRY WITH MINIMAL RISK-FACTOR</i>	40
<i>FIGURE 51: CAMPBELL DIAGRAM AND TIME RESPONSE OF THE GEOMETRY WITH MINIMAL RISK-FACTOR</i>	40
<i>FIGURE 52: RISK-FUNCTION ENVELOPE OF THE GEOMETRY WITH MINIMAL RISK-FACTOR</i>	41
<i>FIGURE 53: FEM ELEMENTS</i>	46

Sommario

L'attività di tesi qui esposta è stata sviluppata all'interno di GE Avio Aero S.r.l., in collaborazione con il Politecnico di Torino.

La tesi ha lo scopo di sviluppare uno strumento per l'ottimizzazione parametrica della geometria delle ruote dentate presenti nelle trasmissioni di potenza dei sistemi propulsivi aerei.

In ambito aeronautico, componenti e ingranaggi devono essere sempre più leggeri e quindi propensi a vibrare. Le vibrazioni forzate in condizioni di risonanza riducono la vita a fatica del componente e quindi attribuirne migliori caratteristiche dinamiche e statiche si scontra con la necessità di un incremento della massa.

Per questo motivo, ci si è posti come scopo la ricerca del miglior compromesso tra i due obiettivi dell'ottimizzazione: minimizzare massa e ottenere migliori proprietà statiche e dinamiche.

Per migliorare il comportamento statico e a fatica della ruota dentata durante l'ingranamento si è scelto di minimizzarne lo spostamento statico e l'ampiezza delle vibrazioni e di spostarne i picchi di risonanza lontano dalle velocità operative, agendo sulla geometria del design space.

Per caratterizzare le risposte all'eccitazione di ogni configurazione e per confrontarle tra di loro è stata definita la funzione *Risk-Factor*, che dà in output un parametro correlato alla presenza di picchi di risonanza all'interno degli intervalli operativi di velocità e allo spostamento statico.

Il tool è stato sviluppato interamente su MATLAB e in maniera tale da garantirne l'applicazione per le diverse tipologie di ingranaggi.

In particolare, in questa tesi sono stati condotti tre test: i primi due con lo scopo di testare il tool su una geometria semplificata e il terzo su una ruota cilindrica a denti dritti.

Abstract

This MSc. thesis has been carried out at GE Avio Aero S.r.l. under a mutual industrial agreement between Politecnico di Torino and the company.

The aim of this thesis is the development of a tool able to optimize the performances of toothed wheels typically employed in the gearbox of aircraft propulsion systems.

According to aeronautical trends, components and gears must weigh less and less so they tend to vibrate. Forced vibrations at resonance conditions reduce the fatigue life of the component and for this reason, to achieve better static and dynamic properties is in contrast with the need to reduce its mass.

For this reason, the purpose of this thesis activity is the search of the best compromise between the two optimization objectives: reduce gear mass and improve the gear response to the excitation.

To ensure a longer fatigue life of toothed wheels it was chosen to minimize the amplitude of static displacements and vibrations and to move away the resonance peaks from the operating speed ranges, leveraging on the available design space.

To characterize the dynamic behaviors of each configuration and to compare them with each other, the function Risk Factor is defined, which gives as an output a factor related to the dangerous presence of resonance peaks inside gear operative ranges and to the static displacement.

The optimization tool has been developed entirely in MATLAB environment and in a generic form, in order to guarantee its application for whatever gear's typology it is wanted to take into analysis. Particularly, in this thesis three tests are been performed: the former test the tool on a simplified geometry and the third is related to a spur gear.

Acknowledgments

Desidero ringraziare l'Ing. Luca Ronchiato, il mio tutor aziendale, che con grande disponibilità mi ha guidato in questi mesi.

Ringrazio il mio relatore, il prof. Daniele Botto, per avermi dato l'opportunità di svolgere la tesi in un'azienda leader nel settore aerospaziale.

Grazie a tutta la mia famiglia, ai miei amici e ai colleghi, per il supporto continuo datomi in questi anni.

Introduction

In recent years, the number of turbine engine-powered aircraft in both commercial and military service has increased. This growing has resulted in an increased interest in reducing air pollution produced by aircraft.

This thesis is part of GREAT 2020 (Great Engine for Air Traffic 2020) project which was born in 2009 and in which is involved a dense network of companies operating in the aeronautical field in Piedmont.

The aim of this research is to develop innovative and environmental-friendly technologies for next-generation aircraft engines.

The combustion process in aircraft engines produces carbon dioxide (CO_2), water vapor (H_2O), nitrogen oxides (NO_x), carbon monoxide (CO), oxides of sulfur (SO_x), unburned or partially combusted hydrocarbons, particulates, and other trace compounds.

The main objectives of GREAT 2020, defined by the European Commission together with a group of experts ACARE (Advisory Council for Aviation Research and Innovation in Europe), concern in a 50% reduction of the CO_2 emission, an 80 % reduction of NO_x emission and a reduction of the perceived noise up to 10 dB in comparison with 2000 technologies.



Figure 1: ACARE objectives

The quantity of CO_2 and NO_x produced is directly proportional to the quantity of fuel burned. NO_x emissions are also related to combustor inlet air temperature: when the temperatures in the

combustion chamber are at the highest level, NO_x emissions are maximum. Thus, the highest levels of emissions are normally generated at full power operating conditions, particularly at takeoff. Therefore, to reduce emissions is necessary to reduce the amount of fuel that must be burned during the operative life of the engine. Thus, it is necessary to increase the overall efficiency of the engine and, on the other hand, to reduce the weight of the aircraft components.

According to these objectives, the aim of this thesis is to reduce the weight of a gearbox wheel, by developing a methodology based on parametric optimization.

The 2d cross section of the wheel are parametrized and the user has the possibility to choose the parameters that the toll will modify, inside the specified ranges of variation, in order to find their optimal values.

1. Literature

Vibration is a mechanical phenomenon whereby oscillations occur around an equilibrium point of the system.

The origin of vibrations has to be found in bodies deformability, in fact bodies are able to storage energy in different forms and the continuous internal exchange of potential and kinetic energy manifests itself with vibrations around an initially equilibrium condition.

Generally, engineers try to avoid vibrations, because they have unpleasant effects: for instance, vibrations may cause fatigue failure, extreme discomfort and unwanted noise pollution or loss of precision in controlling machinery.

Therefore, a careful design is necessary to minimize unwanted vibrations.

In an un-damped system, after that system has been excited, vibration continue to occur for an infinite period, and their natural frequencies are function only of mass and elasticity proprieties of the system. Instead, if in the system are present some dumping effect, the energy of a vibrating system is gradually dissipated, and the vibrations gradually reduce and change in frequency.

Vibration could be forced vibration or free, depending on the existence or not of a continuous excitation source.

1.1 Spur Gears

Spur gear or straight-cut gear consist of a cylinder with teeth projecting radially. This type of gear has straight teeth, and is mounted on parallel shafts, for this reason, no axial force is created by the meshing of the teeth.



Figure 2: Spur Gears

On the other hand, each impact between the teeth makes noises and causes vibration, which is the reason why spur gears are excellent at moderate speeds but tend to be noisy and unreliable at high speeds.

1.2 Helical Gears

The helical or "dry fixed" gears are used in almost all mechanical transmissions. The leading edges of the teeth are not parallel to the axis of rotation and their shape ensure a gradual engagement, that makes helical gears operate much more smoothly and quietly than spur gears. Helix angle can vary from 15 to 30 degrees. The thrust load varies directly with the magnitude of the tangent of helix angle.

The disadvantages of this solution are the production of a resulting force along the axis of the gear, which must be supported by a special ball bearing, and the greater contact surface of teeth that causes greater friction.

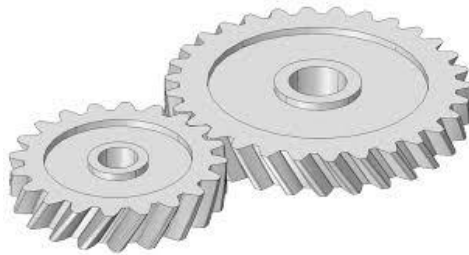


Figure 3: Helical Gears

Helical gears can be meshed in parallel or crossed orientations. The former, the most common orientation, refers to when the shafts are parallel to each other. In the latter, the shafts are nonparallel, and in this configuration the gears are sometimes known as "skew gears".

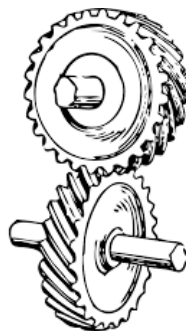


Figure 4: Crossed Helical Gears

1.3 Bevel Gears

A bevel gear is shaped like a right circular cone with most of its tip cut off and is used when the direction of a shaft's rotation needs to be changed. This type of gear can be designed to work at every angle except zero or 180 degrees.

Bevel gears have teeth that can have straight, spiral, or hypoid shape. Each type of tooth has the same pro and cons of cylindrical gear.

For straight and spiral bevel gears, the shafts must be perpendicular to each other, but they must also be in the same plane. Instead the hypoid gears can engage with axes in different planes.



Figure 5: Straight Bevel Gears - Spiral Bevel Gears - Hypoid Bevel Gears

1.4 Worm Gears

A worm gear system consists of a worm and a gear. The worm is analogous to a screw and the gear is a spur gear.

The reduction ratio is determined by the number of starts of the worm and by the number of teeth on the worm gear.

Many worm gears have an interesting property, which is known as self-locking feature: while you can rotate the gear by worm, it is not possible to rotate worm by using the worm gear.

The meshing of the worm and the gear consists of sliding and rolling actions, but sliding contact dominates at high reduction ratios and causes friction and heat, which limits the efficiency of worm gears.

Although their efficiency is relatively low, they are the most compact type of system and they can provide high reduction ratios and correspondingly high torque multiplication.



Figure 6: Worm Gears

2. State of art

Literature offers many approaches to evaluate the dynamic behavior of gears and their design optimization.

Transmission Error (TE) is considered to be the primary cause of noise in Gear Boxes and it is defined as the difference between the ideal relative positions of two unloaded gears, without manufacturing errors, and their relative positions under real operating conditions.

The main causes of transmission error are the deformation of the meshing teeth under the applied load and the assembling and manufacturing errors.

The vibrations originating at the gear mesh, i.e. static transmission error, can be amplified by the dynamics of the gear transmission and they can turn into a bigger vibration called dynamic transmission error.

The difference between Maximum and Minimum of the TE trace is defined as Peak to Peak Transmission Error (PPTE).

The gear designer can reduce transmission error both statically, with opportune profile modifications, and dynamically, by means of an accurate study of the dynamics of the gear transmission.

2.1 Micro-geometrical optimization methods

In the last years, were developed different gears dynamics optimization methods, the majority of which focused on micro-geometrical modifications of the teeth profile of the gear, with the aim of reducing noise since TE can be significantly reduced if an optimized profile modification is produced.

The influence of profile modifications on the dynamic response was proved by Kahraman and Blankenship in their paper “Effect of Involute Tip Relief on Dynamic Response of Spur Gear Pairs” [1].

Most of the design methods are based on the use of tip and root relief, which consist in a removal of material from the tooth flank in order to reduce the fluctuation of the transmission error at the nominal torque level.

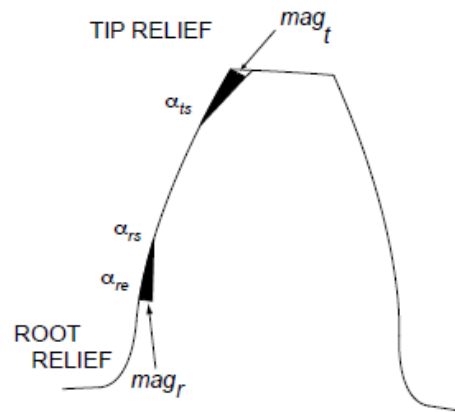


Figure 7: Profile modification parameters

Today there are many theoretical and computational tools which can predict the transmission error of a gear during the design stage. These tools allow the designer to introduce appropriate profile modifications to reduce TE, not empirically, but based on consolidated theories.

2.1.1 A method to define profile modification of Spur Gear

In 2004 Beghini, Presicci and Santus in collaboration with GE AVIO S.r.l. published the paper “A Method to define Profile Modification of Spur Gear and Minimize the transmission Error” [2], in which they proposed an iterative method to reduce the peak to peak Static Transmission Error. They carried out several simulations of meshing gears, combining Finite Element technique with a semi-analytical solution and neglecting rotational speed and inertia forces.

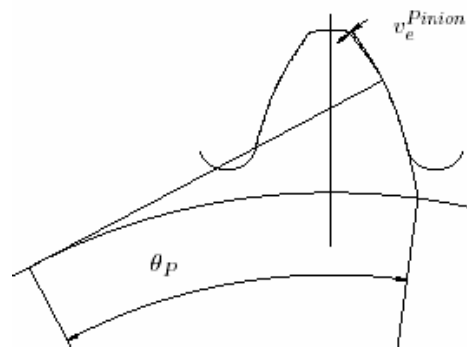


Figure 8: Pinion Tip Relief and Roll Angle

The optimization parameters, that are shown in Figure 8, are the tip relief and the roll angle for each gear.

Tip reliefs are defined as the thickness, v_e , of the material removed along the tooth flank with reference to the nominal involutes profile.

The range of optimization for the Roll Angle are The Start Active Profile roll angle (SAP) and the End Active Profile roll angle (EAP).

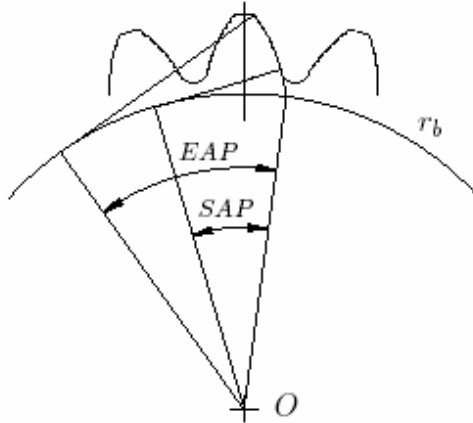


Figure 9: Definition of SAP and EAP

2.1.2 Optimization methods for spur gear dynamics

In 2011, Barbieri, Scagliarini, Bonori, Pellicano and Bertacchi [3] proposed two different approaches for spur gear noise reduction using micro-geometrical modifications. They are based respectively on the reduction of Static Transmission Error (STE), similarly to what Beghini, Presicci and Santus [1] did, and Dynamic Transmission Error (DTE).

The dynamic behavior of the system is computed through a simple lumped parameter model, that is showed in figure 10.

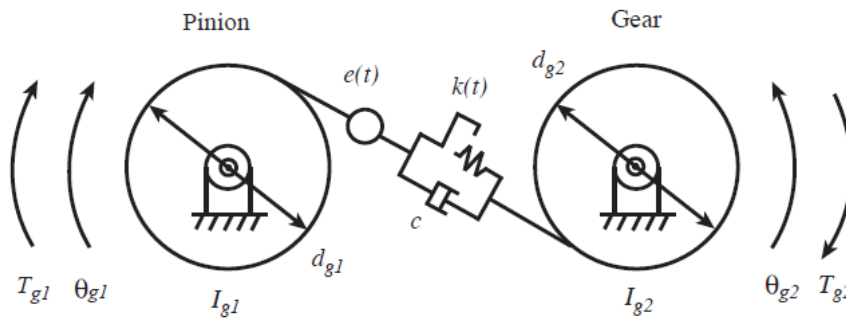


Figure 10: Dynamic Model of Spur Gears

The optimization parameters are the roll angle of start at the tip and at the root and magnitude relief at the tip and at the root. In this way they defined an 8-dimensional parameter space.

However, solutions show that very small modifications at root and since root modifications are more difficult to realize than tip modifications, tip only modifications could be considered.

2.2 Geometrical optimization methods

In order to reduce the mass of gearbox, optimization tools act not only with micro-geometrical optimizations of teeth profile of gears, but also different approaches using geometrical modifications on the entire available design space was developed.

In the next sections two different approaches, that were developed at Politecnico di Torino in collaboration with GE AVIO S.r.l., are presented.

2.2.1 Multi-objective Dynamics Optimization for Aeronautical Gears

In 2017 Luca D'Alò carried out a thesis work on the “Multiobjective Dynamics Optimization for Aeronautical Gears” [4].

He developed an optimization tool that could be used to optimize the design of any type of gear, minimizing the frequency response in the operative ranges.

In his work he modeled the geometry to be optimized with parametric curves and, in particular, he used two Bezier curves.

In this way the toll creates different configurations acting on the positions of the poles and on its weights, that are the optimization parameters.

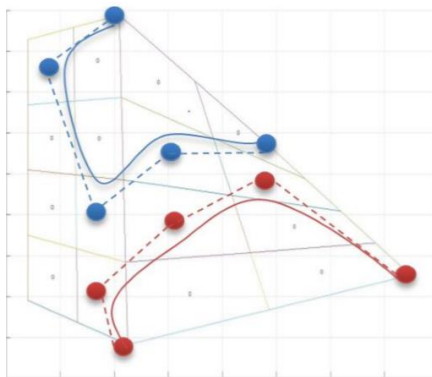


Figure 11: Bezier Curves

2.2.2 Static and Dynamic Topology Optimization

In 2018 M. Casiello in her master's thesis "Static and Dynamic Topology Optimization for Aeronautical Gears" [5] shows that is possible to implement in Optistruct working space gear design optimizations.

The method developed in this thesis falls in the field of topology optimization and performs static and dynamic analysis.

The optimal configuration that was found has the most efficient material distribution in the design space, minimizing the compliance and respecting static requirements.

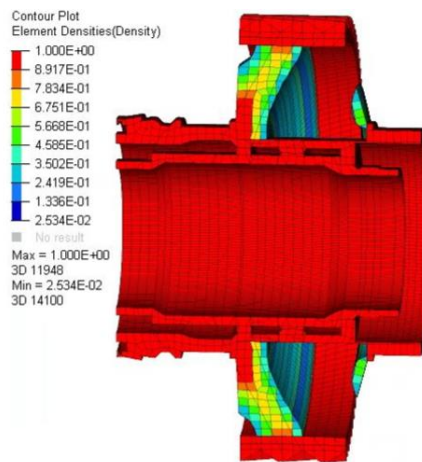


Figure 12: Topology optimization

3. Tool structure

Tool architecture can be decomposed in three black boxes:

- The meshing program, that discretizes the gear section;
- The time response and mass calculator;
- The optimizer, which for each iteration compares the new outputs of the previous black box with the old ones and generates the set of parameters that define the next geometry to be analyzed.

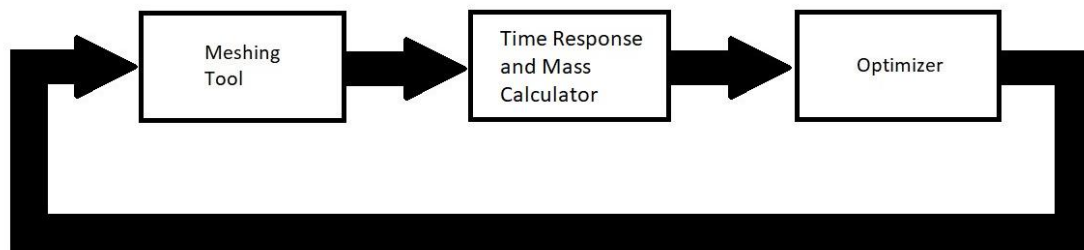


Figure 13: Representation of the Tool structure

3.1 User Inputs

The inputs that the user will have to set are presented in this section.

In the input parameters template, that is called “dati_input”, the user must define:

- The geometry of the initial cross-section of the gear. It is defined, in matrix form, by points coordinates and lines. It is also necessary to specify which is the area to optimize, the design space, and which are the fixed ones, the no-design space. The design space is defined as a function of the optimization parameters;
- The optimization variables, that are the parameters that the optimizer could modify, and which are used to define the design space;
- The ranges of variation of the optimization parameters, i.e. the minimum and maximum values that each parameter can assume;

- The materials properties and the material of the different areas;
- The parameters of the gear, including number of teeth, pitch radius and pressure angle;
- The operative conditions, in terms of operative angular speeds and applied loads.
- Constrains and forces. It must be specified how many degrees of freedom the constrained nodes have and direction and amplitude of the excitation forces.
- The functions to be optimized. As default setting, they are the mass function and the risk factor function.
- The weights vector, that indicates the relative weights of the objective functions.
- The options structure for the optimizer (tolerance, maximum number of iterations and length of the steps).
- The options for the dynamic analysis (the mesh parameter, the number of modes to be computed and the sampling rate).
- The outputs folder, in which the results are saved.

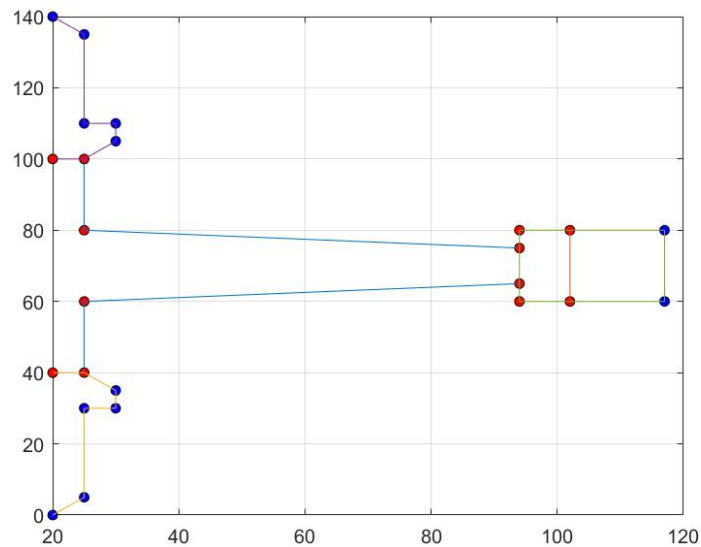


Figure 14: Example of geometry input data

3.2 Toll outputs

The tool will return the design parameters, the mass, the risk factor and the value of the weighted objective function of each analyzed configuration. These data, the dynamic response and the Campbell diagram of each configuration are saved in the specified output folder.

The tool is also able to plot and animate the 3D expansions of mode shapes.

Another result of the optimization process is the Pareto diagram, in which the best solution is put in evidence.

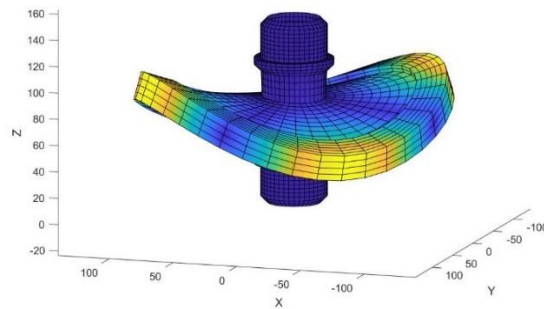


Figure 15: Example of mode plot

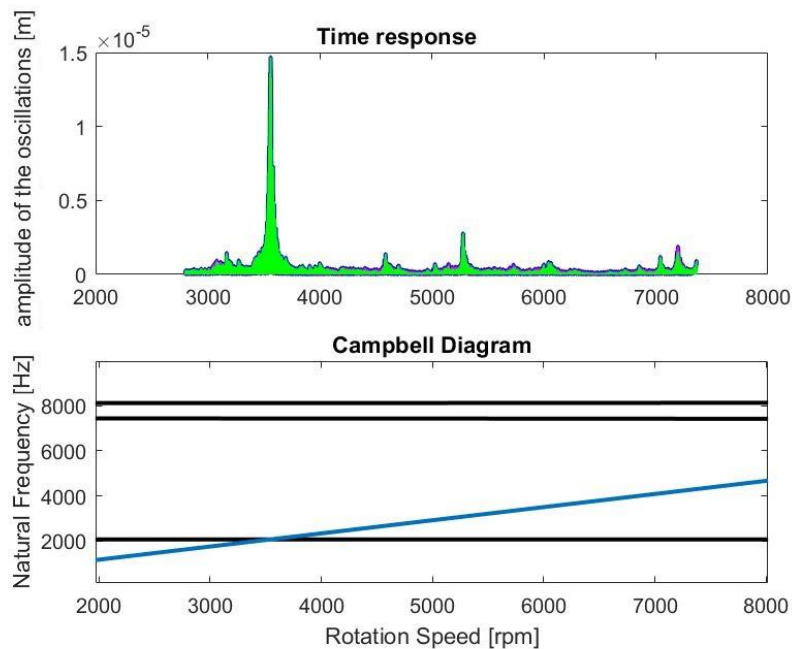


Figure 16: Time response and Campbell diagram

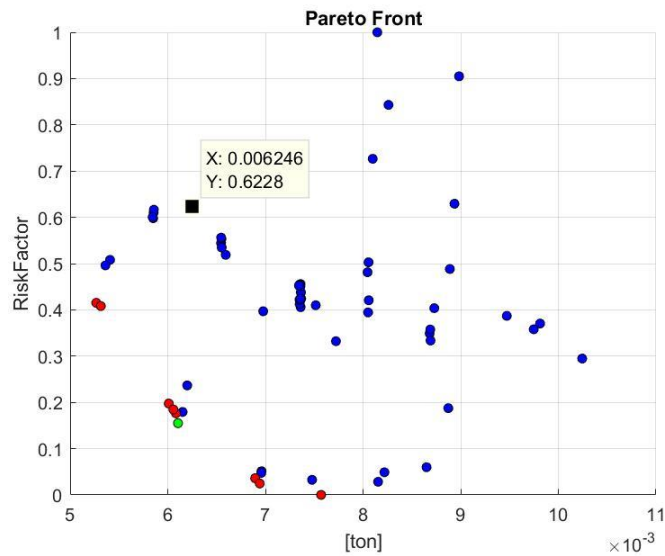


Figure 17: Pareto front

3.2.1 Pareto Front

Fig.17 shows the values of the objective functions computed in different sample points, on which the points which belongs to the Pareto front are marked in red.

The Pareto front gives information about how improving one objective is related to deteriorating the second one. For this reason, it is also named tradeoff curve.

Therefore, these points represent the best parameters configurations from which is possible to choose the optimum condition depending on user input. In fact, the weights to give to the mass and to the risk factor depend on the gear application.

Points of Pareto front are characterized to be Pareto optimal and the other points are called Pareto dominated.

One point is Pareto optimal if no objective function can be improved without deteriorating another. Since a designer can make tradeoffs within this set of points, rather than considering the full range of each parameter, the Pareto front is particularly useful in engineering.

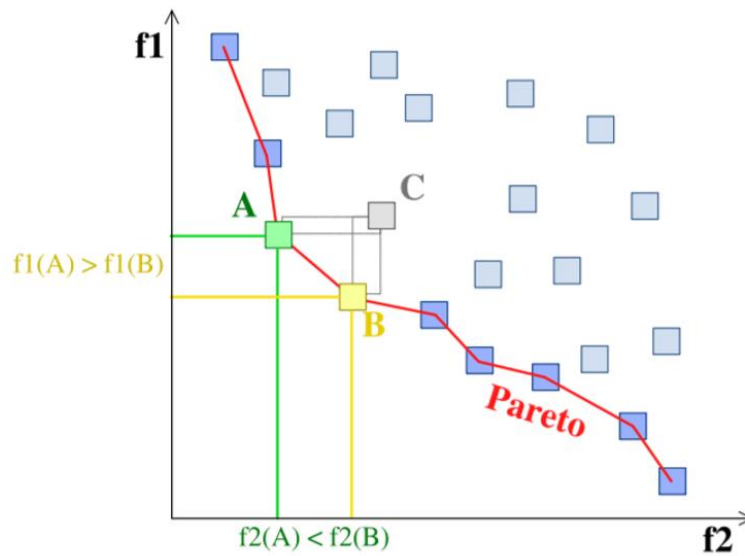


Figure 18: Representation of Pareto Front

3.3 Design space definition

One important step in geometry optimization is the definition of the design space, i.e. the parts of the gear that are designable during the optimization process.

In the gearboxes design there are parameters that cannot be modify for functional reasons or because legislation impose it.

Thus, the developed tool distinguishes the Non-Design Space and the Design space.

The gear meshes with another one and this is the reason why the teeth geometry cannot be modified. The thickness of the rim it's also considered to belong to the Non-Design Space, because its value follows the standard and must be greater than 20% then tooth's height.

Other limitations are due to the shaft and to the bearing shoulders.

Fig. 19 shows the sections of the mentioned areas and indicates with the number 5 the design space while the other areas represent bearing guides, rim and teeth.

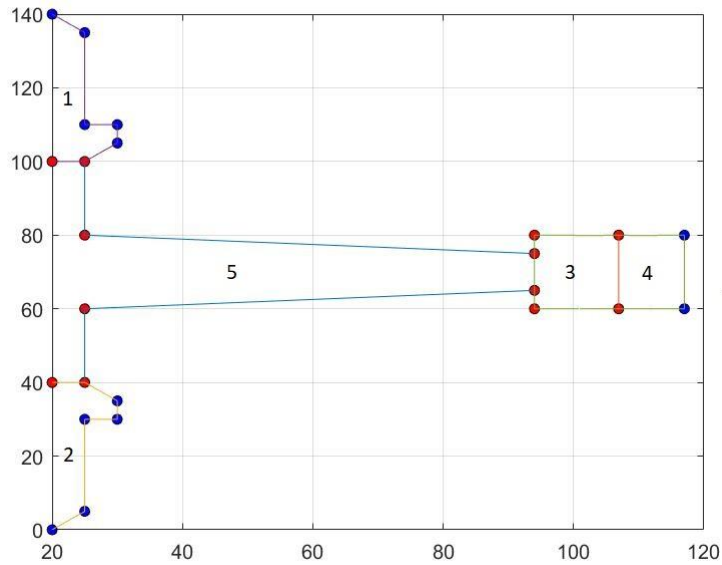


Figure 19: Design and Non-Design spaces

3.4 Mesh generation

The first step of the static and dynamic analysis is the discretization of the two-dimensional cross section of the gear.

The meshing program used in this thesis is a custom meshing tool, developed by an engineer of Politecnico di Torino during his master's degree thesis [7].

The mesh generation algorithm developed in the previous cited thesis consist in two main steps. The domain is initially discretized by triangular elements, through an algorithm called Delaunay triangulation. Then these triangles will be converted to first order rectangular shell elements by a series of geometric operations and transformations, known as Q-morph algorithm.

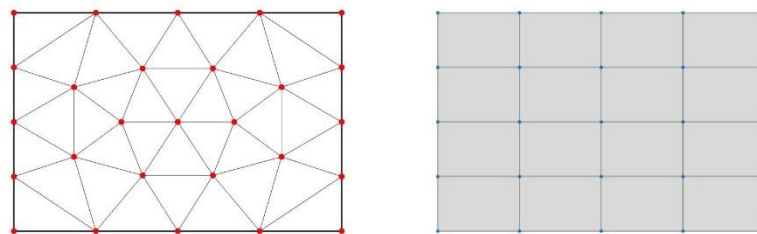


Figure 20: First step of mesh generation

In order to perform a more detailed analysis, for each element four mid-sides nodes and one node in the middle of the face are added.

Thus, the final mesh consists of rectangular second order serendipity elements.

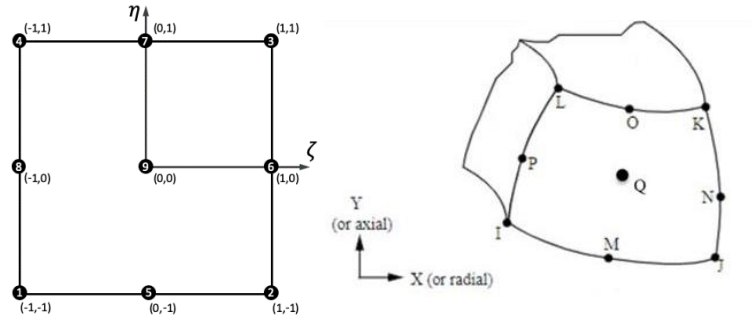


Figure 21: Serendipity axisymmetric element

The performed algorithm starts from placing nodes on the boundary. The user can place the boundary nodes by hand, but in the developed code this action is automatically performed by the function “bound”. The user can control the mesh size through the mesh parameter that defines the maximum length of the edges in which the boundaries are subdivided.

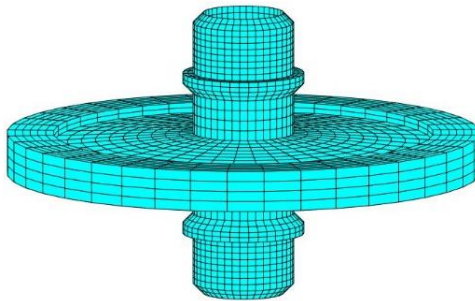


Figure 22: 3D expansion of the 2D mesh

The meshes of Non-Design space areas are the same for all the analyzed geometries thus they can be computed once at the start of the optimization process.

Since bearing guides and teeth belong to Non-Design space, forced and constrained nodes do not change for each analysis and can be defined as initial parameters. Fig.23 puts in evidence these nodes.

As typically rule in gear design, it is supposed that a radial and an axial and radial bearing are mounted between the shaft and gear. For this reason, one set of constrained nodes, referred to the

radial and axial bearing, has only the tangential degree of freedom, while the other set also has the axial one.

Figure 23 also shows an example of domain discretization. It can be seen that some elements of the mesh are distorted, but since a transient analysis will be implemented, we are focused on the overall behavior of the system. Therefore, the presence of some distorted elements can be accepted.

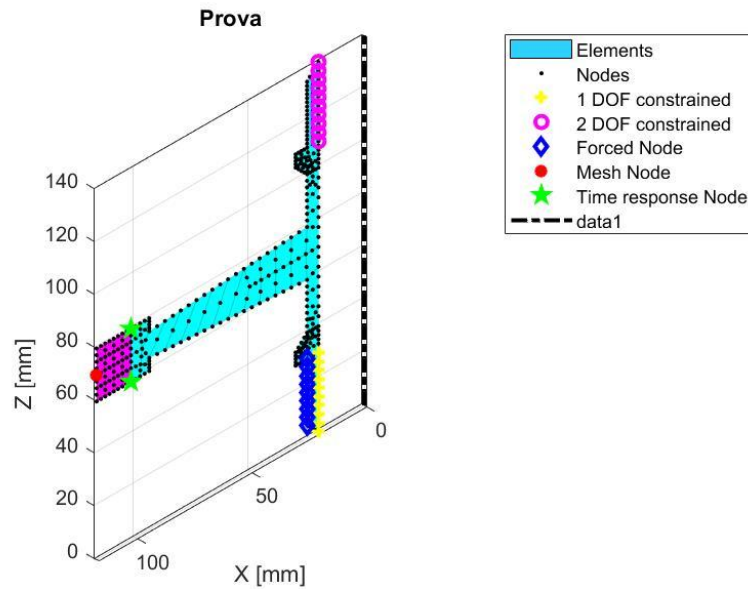


Figure 23: Mesh, constrained and time response nodes

3.5 Time Response Analysis

The time response analysis is computed in MATLAB environment using a GE-AVIOAERO code.

Through the expansion of the two-dimensional cross section with Fourier series, the tool is able to compute the dynamic response of any axisymmetric structure.

The properties of a mechanical system can be described by Stiffness \mathbf{K} , Mass \mathbf{M} and Damping \mathbf{C} . In the case of rotordynamics, also the gyroscopic matrix \mathbf{G} must be considered. It contains inertial terms that are strictly linked with the gyroscopic moments acting on the rotating parts of the machine.

Thus, the dynamic system can be described by the matrix equations:

$$\underline{\mathbf{M}}\ddot{\mathbf{q}} + \underline{\mathbf{\Omega}} \underline{\mathbf{G}}\dot{\mathbf{q}} + (\underline{\mathbf{K}}(\boldsymbol{\theta}) - \underline{\mathbf{\Omega}}^2 \underline{\mathbf{C}})\mathbf{q} = \mathbf{f} \quad (3.1)$$

Where \mathbf{f} is the external forcing term and \mathbf{q} , $\dot{\mathbf{q}}$, and $\ddot{\mathbf{q}}$ are the generalized displacements, velocities and accelerations. In the stiffness matrix is also considered the contribute of the mesh stiffness, that change in time with a low defined over the angle $2\pi/z$, where z is the number of teeth, and therefore the stiffness matrix is a function of the tangential coordinate.

In order to explore the dynamic behavior of the gear in the whole operative speed range a speed sweep is performed.

Since time domain analyses are time intensive the displacements of the nodes are computed only in the operative speed ranges and the static displacements are calculated as middle values of all displacements registered.

The nodes of which time responses must be computed can be selected by the user and they must be specified in the variable "TimeNode". As forced and constrained nodes, the time nodes positions are fixed and can be defined in the input parameters template.

To correctly evaluate the distortion of teeth, the two nodes must be located on a tooth and on the opposite faces of the gear, as it is shown in Fig.23.

The following equation guaranties that the optimized component will not allow a static torsion greater than a certain tolerance.

$$|\mathbf{U}_{A,static} - \mathbf{U}_{B,static}| \leq \mathbf{tolerance} \quad (3.2)$$

Where $\mathbf{U}_{x,static}$ are the static displacements vector of components \mathbf{u}_r , \mathbf{u}_θ and \mathbf{u}_z , which are the displacements in the radial, tangential and axial directions.

It's also necessary to avoid great absolute radial and axial displacements of the teeth. For this reason, also the following equations must be satisfied.

$$|\mathbf{u}_{r,static}| \leq \mathbf{tolerance}' ; |\mathbf{u}_{z,static}| \leq \mathbf{tolerance}'' \quad (3.3)$$

The values of the tolerances are to be set in the variables "rot0" and "sp0".

3.5.1 Nyquist Theorem

To correctly describe the system's response an adequate sampling rate must be settled, i.e. the Nyquist theorem must be satisfied.

The Nyquist rate specifies the minimum sampling rate that enables the signal's accurate reconstruction from the samples.

$$f_{sampling} \geq 2 * f_{signal} \quad (3.4)$$

The theorem can be applied to the studied system, in order to determine the maximum time step that can be used to compute an accurate time response to the meshing force.

The frequency of the meshing force is described by the equation 3.5:

$$f_{Mesh} = z * \Omega \quad (3.5)$$

Where z is the number of teeth and omega is the gear's speed.

Therefore, the Nyquist frequency and so the maximum sampling time for this problem are:

$$f_{Min} = f_{Nyquist} = 2 * z * \Omega ;$$

$$\Delta t_{max} = \frac{1}{f_{Nyquist}} = \frac{1}{2 * z * \Omega} \quad (3.6)$$

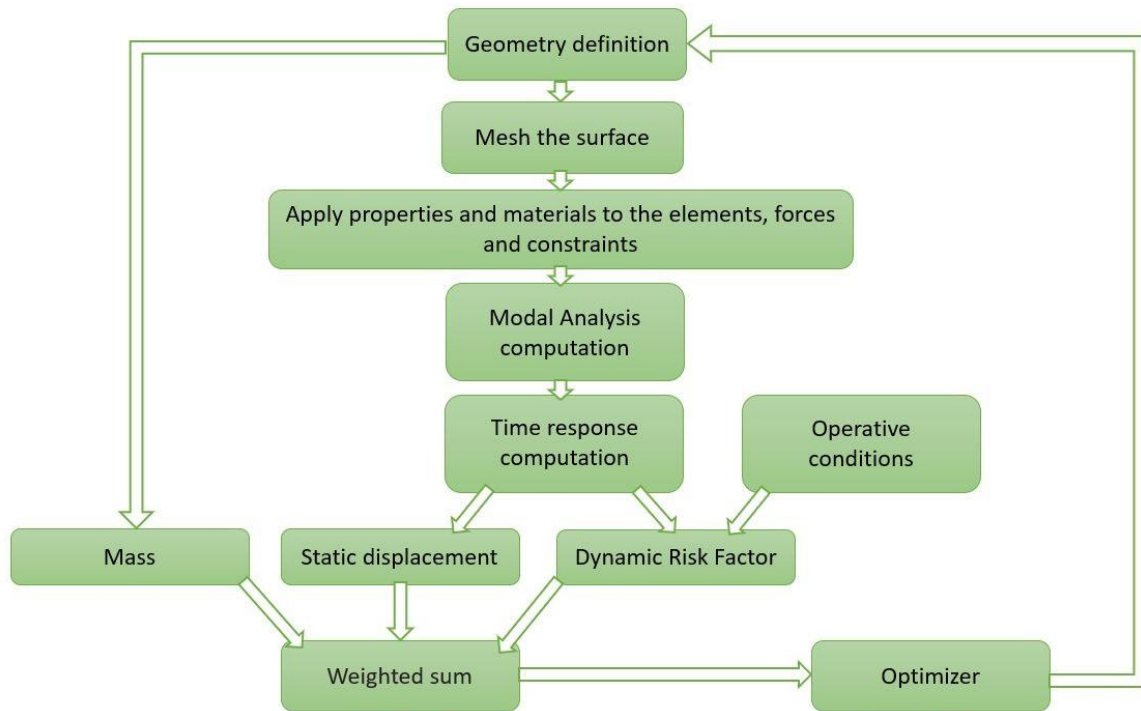


Figure 24: Flow chart of the second black-box code

3.6 Campbell diagram

The Campbell diagram of each configuration analyzed is plotted and saved.

In the Campbell diagram, the evolution of the natural frequencies in function of the rotation speed of the shaft is traced.

Rotors are subjected to forces that vary in time and sometimes their time history is harmonic. The frequency of the forcing function or of its harmonic components is often linked with the spin speed of the rotor and can be plotted on the Campbell diagram. The intersections of the curves related to the natural frequencies with those related to the forcing frequencies identify the critical speeds of rotors.

3 - Tool structure

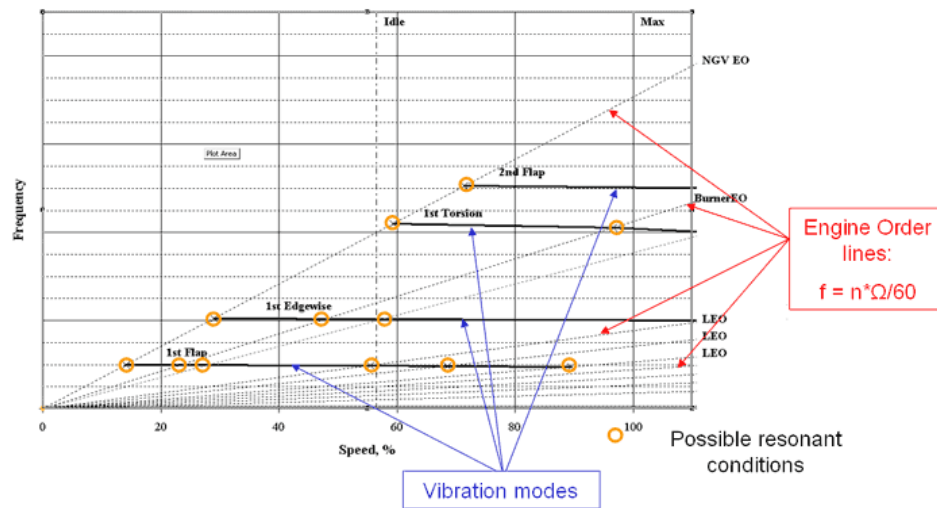


Figure 25: Representation of EO excitations on Campbell Diagram

Not all these intersections on the diagram are dangerous. If the frequency of a forcing function coincides with the natural frequency of a mode uncoupled from it no resonance occurs or the damping of the system can hide the weak resonant peak.

During the gears meshing, there is an exchange of force. Since the contact point moves and the mesh force act in a certain point after a period, the mesh force is harmonic. The frequency at which contacts happen depends on the operating speeds Ω , on the number of teeth z and on the Engine Order n and it is called mesh frequency.

$$f_{mesh} = n * z * \Omega [Hz] \quad (3.7)$$

When forward and backward curves of an excited mode intersect the mesh frequency, resonance happens.

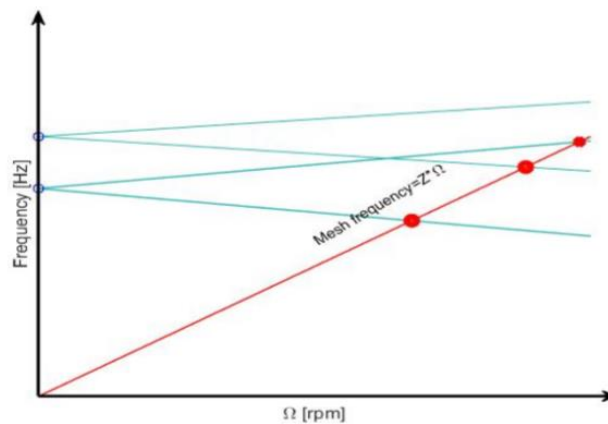


Figure 26: Example of investigation of possible resonance points

3.7 Optimization process

In this thesis work a parametric multi-objectives optimization problem is carried out, because it is desired a final design that is both light and rigid. Since the objectives conflict and considering that it is quite impossible to find the perfect solution that simultaneously presents the optimum condition for all the objective functions, a trade-off must be created.

Between the several optimization algorithms that could be used, the Gradient Descent method was performed.

Although this is a single-objective optimization method, it can be applied by summing the two objective functions. The sum is a weighted sum and the weights of the objective functions can be decided by the user, based on the application of the gearbox.

For example, in aeronautical application, to reduce fuel consumption is used to give preference to mass reduction at the expense of stiffness reduction. On the contrary, if the gear is part of a power plant it is usually preferred a stiffer, but heavier design, because it guarantees a longer gear's life.

The application of the Gradient Descent method starts from specific point, which are chosen between the Latin Optimal Hypercube Sampling outputs.

3.7.1 Latin Optimal Hypercube Sampling

Optimization methods normally are very time consuming. This time depend on the complexity of the problem, but also from the starting point of the algorithm. For this reason, is important to sample the parameters space in order to find the best points of this space from which launching the gradient optimization method. The LOHS used in the tool have been previously generated, using a specific GE AVIOAERO program.

The Latin Hypercube Sampling is a statistical method for generating a near-random sample of parameter values from a multidimensional distribution.

A square grid of sample positions is Latin if and only if there is only one sample in each row and each column. A Latin hypercube is a generalization of this concept to an arbitrary number of dimensions space, in which exist only one sample for each hyper-plane aligned with the Cartesian axis.

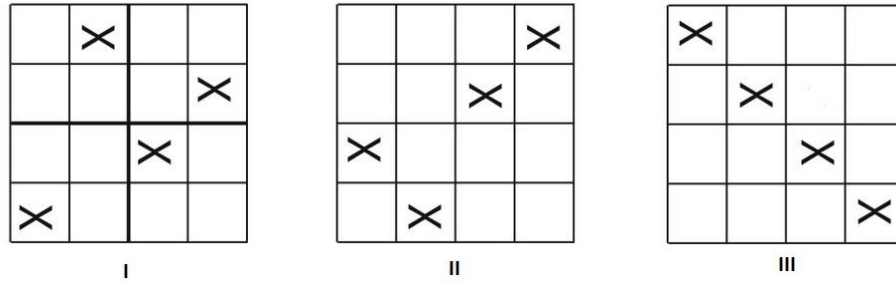


Figure 27: Example of three Latin 2D sampling

To represent the whole parameters space is very important to choose a set of points enough numerous and, above all, well distributed. Thus, between all the possible combination of LHS, only the optimal ones, i.e. with maximum filling propriety, can be used for this thesis scope.

To better explain this propriety, Fig.28 shows two extreme conditions of a 2-dimensional sampling.

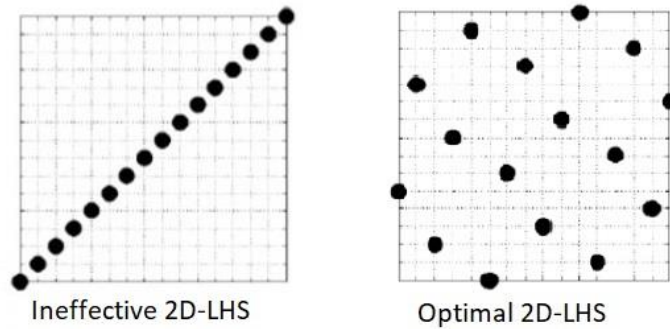


Figure 28: Ineffective and optimal LHS

3.7.2 Gradient Descent Method

The Gradient Descent method is a first-order iterative optimization method for finding a local minimum of a function.

Since it is an iterative method, the value of the objective function is computed in different points, i.e. different values of optimization parameters, and the algorithm defines the rule to move from a point $x(k)$ to the next one $x(k+1)$.

This rule can be expressed by the following equation:

$$\mathbf{x}^{(k+1)} = \mathbf{x}^{(k)} + \mathbf{t}_k \Delta \mathbf{x}^{(k)} \tag{3.8}$$

Where \mathbf{t}_k is the length of the step and $\Delta \mathbf{x}^{(k)}$ is the direction of the k-th iteration.

In the steepest descent algorithm at each iteration the direction is the steepest direction that can be taken to find the minimum. Since the gradient is the direction of fastest increase of the function, this direction is represented by the opposite of the direction of the gradient computed at the point $x^{(k)}$.

$$\Delta x^{(k)} = -\nabla f(x^{(k)}) \quad (3.9)$$

In this way the solution moves towards the nearest local minimum point until reaching it.

The gradient is computed resorting to the finite difference method: the first derivative of the function f at the direction i can be calculated by applying the definition of derivative, which see it as the incremental ratio at the limit and the limit can be approximated with a little step.

$$\frac{\partial f(x^{(k)})}{\partial x_i} = \frac{f(x^{(k)} + h * e_i) - f(x^{(k)})}{h}, i = 1 \dots n \quad (3.10)$$

Where e_i is the unit vector coupled with the i -th direction, h is a little scalar step and n is the number of coordinates in the parameters space, i.e. the number of optimization parameters.

In order to not converge in a local minimum, the method is applied starting from different and well-spaced points, which are chosen from the LOHS sampling points.

The gradient optimization ends when a local minimum will be found or when one of the new parameters of the configuration, that will be analyzed, will exceed its boundary.

3 - Tool structure

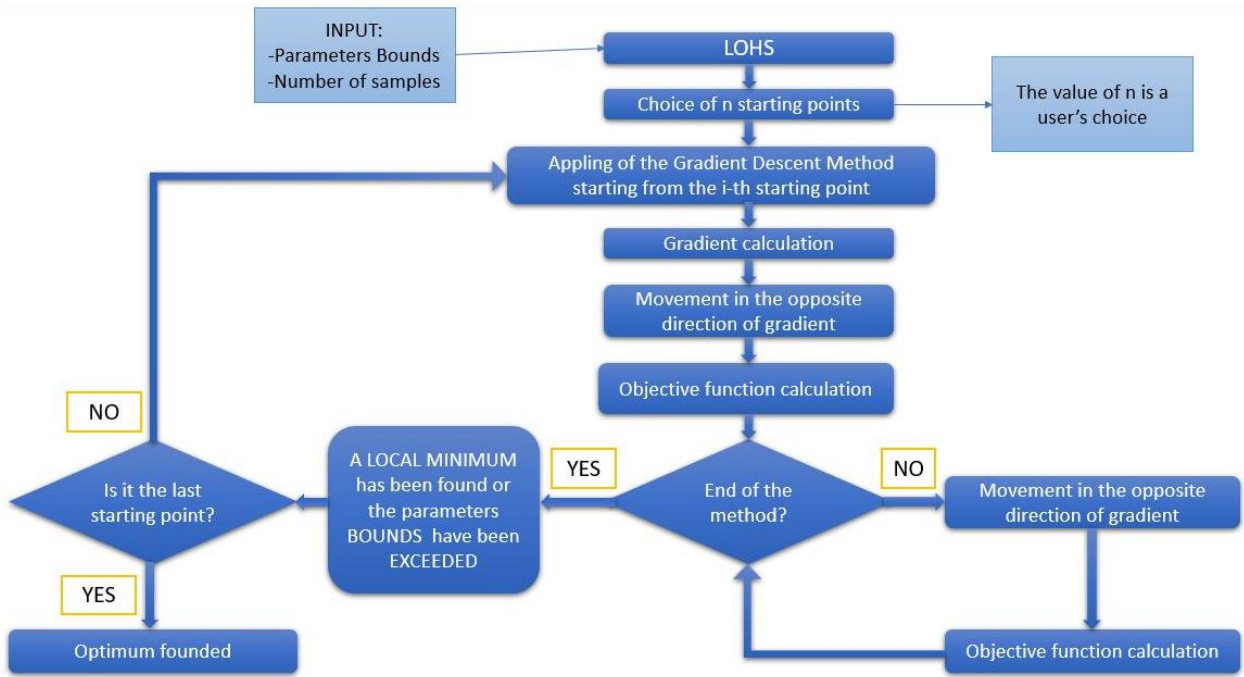


Figure 29: Flow chart of the optimization process

4. Objective functions

Since objective functions definition is the core of the tool, it was considered appropriate to write a chapter devoted to these.

Our objective functions are related to:

- The mass of the structure;
- The Risk-Factor.

As already said in the previous chapter, both these functions need to be minimized and come into a single function obtained by their weighted sum.

Both the objective function approximates the 3d expansion of the gear as a solid of revolution, instead of considers the toothed surface. However, the error resulting from this assumption can be considered negligible.

4.1 Mass Function

The inputs of the mass function are the density, ρ , of the materials the gear is made of and the coordinates of the points defining the section of the gear. The output is the mass value of the whole gear, calculated as a solid of revolution.

If n different materials need to be applied the cross-section can be split in n different volumes, V_i , and the mass of the entire gear is computed by summing the ones related to its subparts.

$$Mass = \sum_{i=1}^n \rho_{(i)} * V_{(i)} \quad (4.1)$$

4.1.1 Pappus-Guldin Second Theorem

The volume V of the gear, or of its subparts, it was computed resorting to the second Pappus-Guldin theorem.

It states that the revolution solid generated by rotating a plane figure about an external axis has a volume V equal to the product of the area A and the distance d , that is equal to the length of the curve traced by the geometric centroid of the plane figure during the rotation.

$$\mathbf{V}_{(i)} = \mathbf{A}_{(i)} * \mathbf{d}_{(i)} \quad (4.2)$$

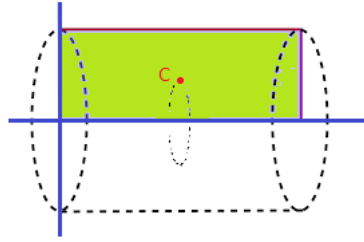


Figure 30: Solid of Revolution

4.2 Risk-Factor function

It is desired to avoid resonance peaks or at least to reduce their amplitudes in all engine operative conditions, as like during Takeoff, Climb, Cruise and Approach.

For this purpose, it is needed to define a parameter that summarizes the static and dynamic behavior of gear. The searched parameter is the Risk-Factor.

The Risk-Factor function implemented in this thesis starts from the one implemented by Luca D'Alò, during his thesis work [4].

In order to explore the dynamic behavior of the gear in the whole operative speed range a speed sweep, from the lowest to the highest speed of operative ranges, is performed and the time response of two nodes is measured. The time response computation is discussed in Section 3.5.

First of all, it is important define which are the factors that have to be taken into account to best characterize the gears response.

The most influential factors are:

1. Peaks of resonance distance from operative conditions

Since peaks outside the operating ranges are not considered dangerous, the system response is calculated only close to the operative speeds. The maximum risk is assigned if the peak is within the operating range and decreases linearly to zero when it is outside a margin range.

2. Load applied in each operative condition

The time response is computed applying the maximum torque at each speed. In this way the response of the system in the ranges in which a lower torque is applied is amplified.

For this reason, the risk is rescaled using the torque values of each speed range to give less importance to the peaks situated in the lower torque ranges.

3. Peaks of resonance amplitude

The amplitudes of the peaks are scaled by setting an upper and lower threshold value to which to assign the amplitude 0 and 1 respectively.

4. Total number of peaks inside the operative range

Since the risk is also related to the number of total peaks in a range, it increases as the number of peaks increases.

5. The maximum static displacement

To obtain an optimal response the static behavior must also be considered during the design optimization.

The maximum static displacement of the nodes it was considered as comparison parameter between the different static response obtained from different cross-section geometries.

However, the tool rejects each configuration that shows static displacements greater than defined threshold values.

The five terms constituting the risk factor could be combined in different ways, for example by summing them, by multiplying them or by computing the average value.

D'Alò found two main formulation to reduce the total risk:

- Minimize only one of the four components;
- Minimize simultaneously all its component.

Using the first formulation the optimizer has more freedom and it can move easily towards zone of minimum risk, but the risk of remaining trapped in local minimum is high.

Using the second formulation, if one parameter tends to zero while another tends to one, the total risk could not change, therefore the optimization could be limited.

In this thesis the risk-factor value is the result of a pondered sum of two terms: the first one deriving from the first four influencing parameters, and so considering the optimization of the dynamic behavior, and the second related to the last parameter, and therefore to the static analysis.

Thus, the user can give a different weight to the static and dynamic contribution.

To insert the first two influential factor into the risk-factor formulation, a function named “risk” is developed.

The risk factor function is defined for all the speed and can vary between zero and one.

For each range of working speed of the engine it can be identified:

- An operative speed
- A margin band
- Two safety bands

The margin band contains the speeds near the working speed and here the risk is maximum for the working range and its value depends on the specific load applied.

The safety bands are composed by the speed near the upper and the lower limit of the range, here the risk function grows linearly from zero to the value of the risk in the margin band.

Thus, for each operative condition the risk shape is trapezoidal and if an operative speed is near to another, its margin band or its safety band could overlap the other operative speed bands. In this case the function calculates the envelope of the two trapezoidal shapes.

Fig.31 shows an example of the shape of the risk function.

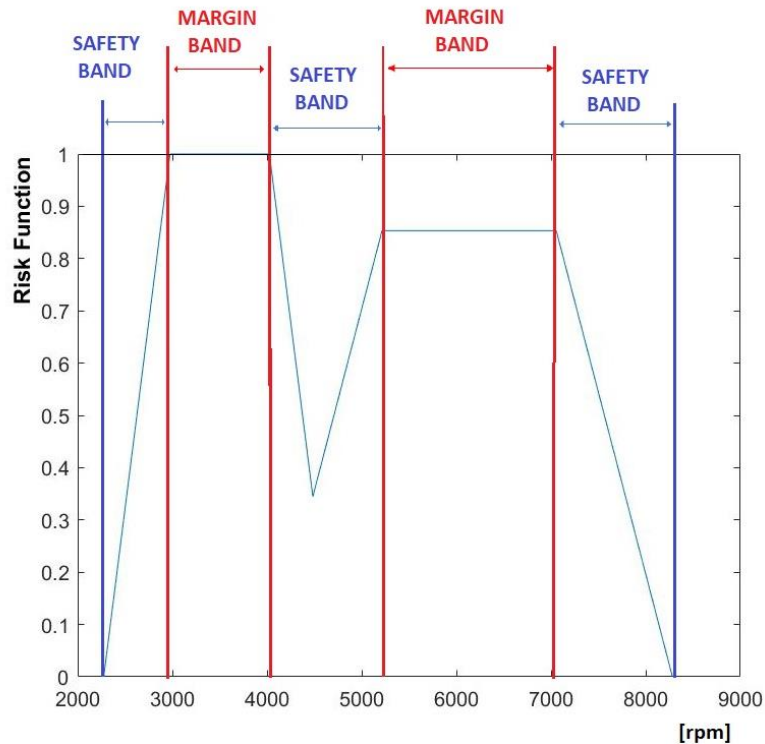


Figure 31: Risk Function envelope

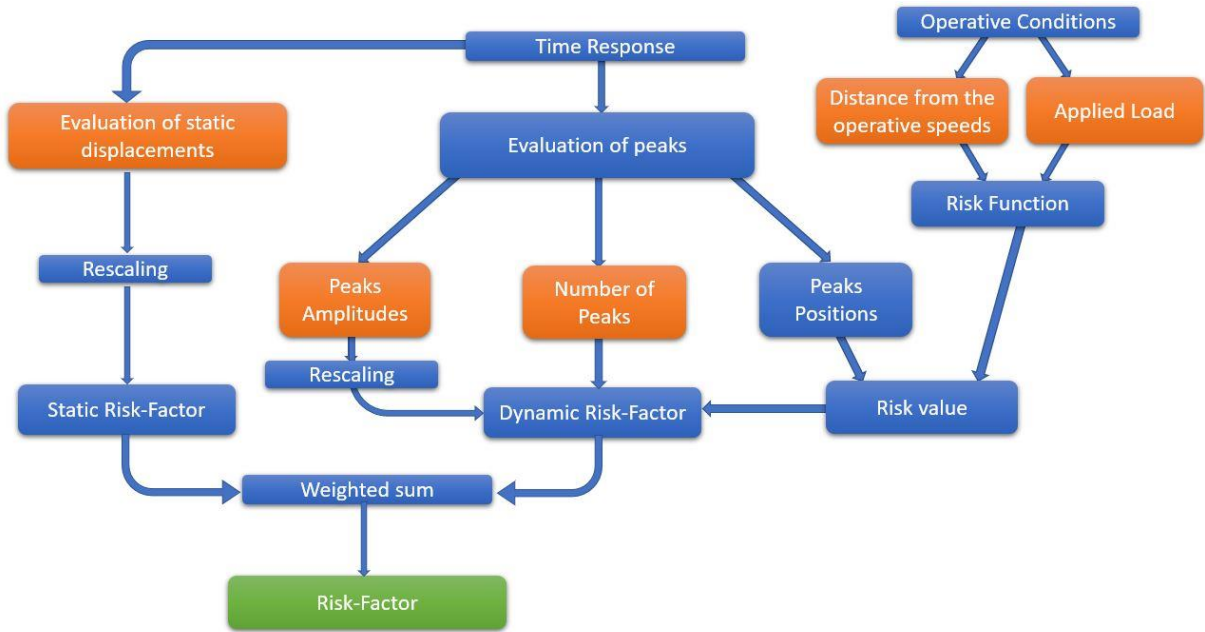


Figure 32: Risk-Factor formulation

After that all the terms influencing the Risk-Factor have been explained it is possible to write its mathematic equations:

$$\mathbf{RiskFactor} = \mathbf{RiskFactor}_{Dynamic} * \mathbf{w}_D + \mathbf{RiskFactor}_{Static} * \mathbf{w}_S \quad (4.3)$$

Where \mathbf{w}_D and \mathbf{w}_S are the weights of the dynamic and static factor respectively, which are chosen by the user, and:

$$\mathbf{RiskFactor}_{Dynamic} = \sum_{i=1}^n \mathbf{PeakAmplitude}_{(i)} * \mathbf{Risk}_{(i)}; n = \mathbf{PeaksNumber} \quad (4.4)$$

$$\mathbf{RiskFactor}_{Static} = \max(\mathbf{axial\ displacement}, \mathbf{radial\ displacement})_{rescaled} \quad (4.5)$$

5. Two-Parameters Optimization

Since only in a 2D parameter space it is possible to graphically visualize all the results useful to better understand the functioning of the tool, firstly test cases in a 2D parameter spaces are carried out.

The first test case consists on a ring with a rectangular cross-section, that basically represents only the RIM and the toothed parts of a gear.

Therefore, As Fig.33. shows, the section is defined by only two parameters: face-width and RIM height.

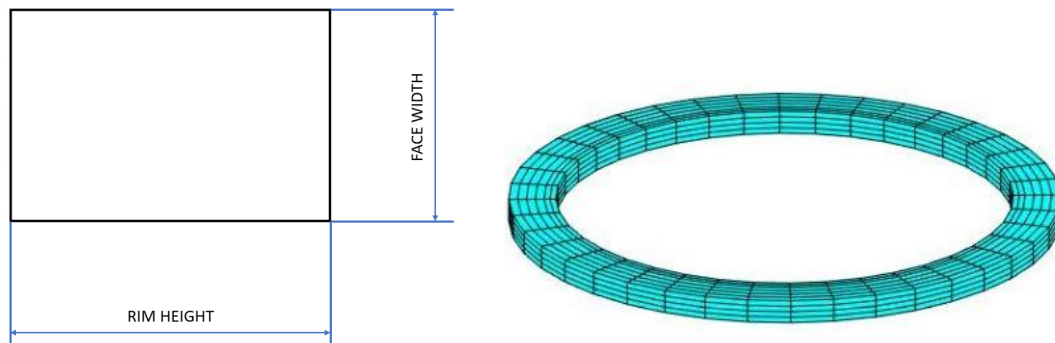


Figure 33: Simplified geometry section and 3D expansion

Then a second test was performed on the complete geometry section of a spur gear, varying only the thickness in the internal and external radius of the Design-Space.

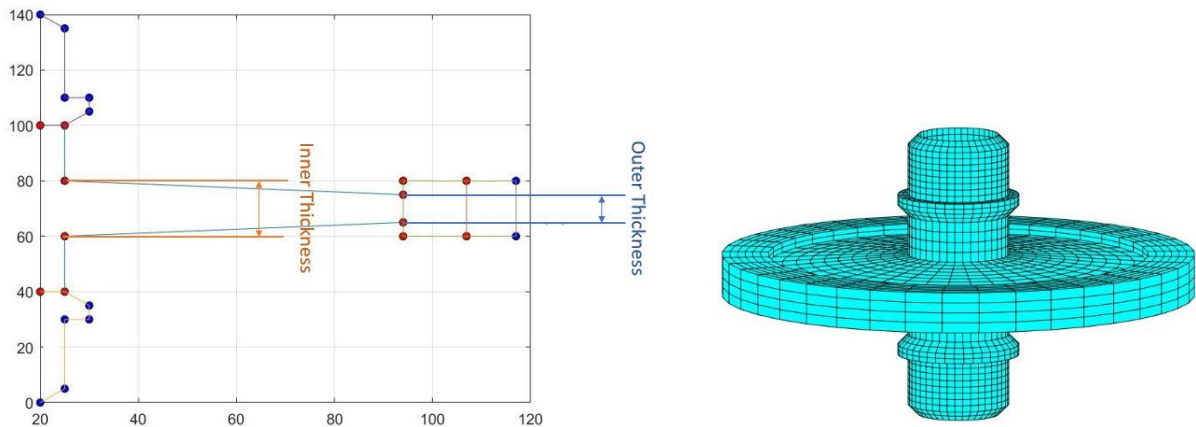


Figure 34: Two-Parameters Optimization Gear Section

5.1 Results validation

Both the tests were performed applying the same operative conditions, in terms of angular speed and applied torque. In particular, the designs were optimized in two operative ranges:

OC 1: 3500 rpm – 341 N/m

OC 2: 6135 Rpm – 291 N/m

To test the tool's capability to search the optimal condition, large ranges of variation of the parameters were fixed.

5.1.1 CASE 1 - Ring

As Fig. 35 shows, the mesh excitation was applied on the outer radius in the center line of the rim and the axial and radial displacements of the nodes on the inner radius were locked.

Since it was chosen to excite in both radial and axial directions, a helix angle has been set for the teeth.

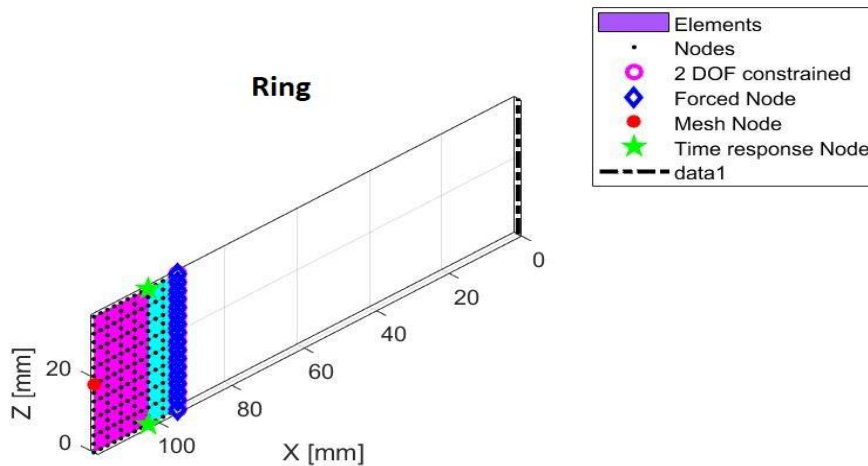


Figure 35: Representation of forces and constrains of Test Case 1

It can be noticed that, since the geometry is simple, the generated mesh by the q-morph tool is regular for all the parameter sets.

5. Two-Parameters Optimization

In order to analyze objective functions shapes, an interpolation has been performed, and the results are represented in the figure 36, in which the mass, the Risk-Factor and the objective functions are plotted.

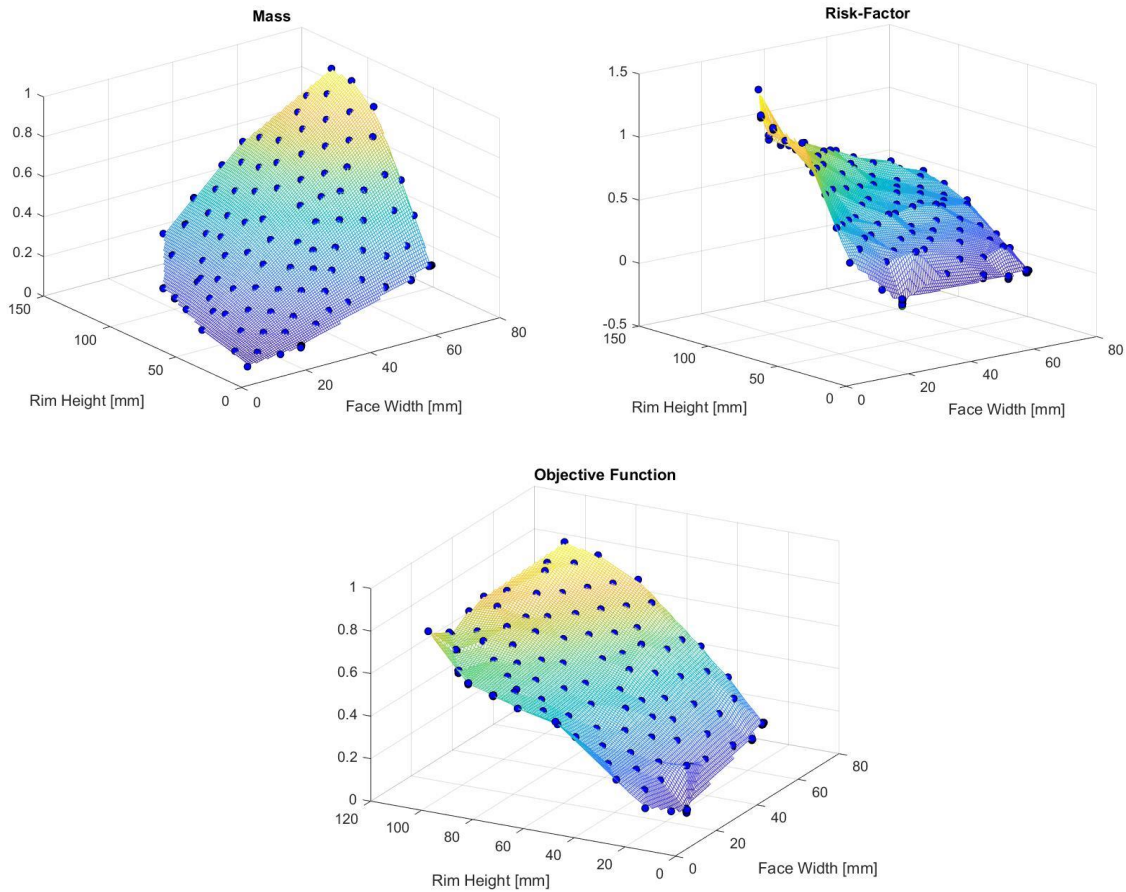


Figure 36: CASE1 – Plot of Mass, Risk-Factor and Objective Functions

As can be noticed looking at the results plot in Fig.36, all functions show the same trend, the functions decrease with decreasing the section parameters.

If this trend is obvious for the mass function, it can appear atypical for the Risk-Factor, since an increasement of rigidity with the increasing of the section area could have been expected.

However, it can be explained noticing that the constrains move towards the external radius with reducing the rim height, and it increases the rigidity of the system.

Therefore, in this case, the optimal parameter setting coincide with their minima.

Figure 37 shows the values of the objective functions for all the configuration analyzed and the Pareto front that derives from the optimization process.

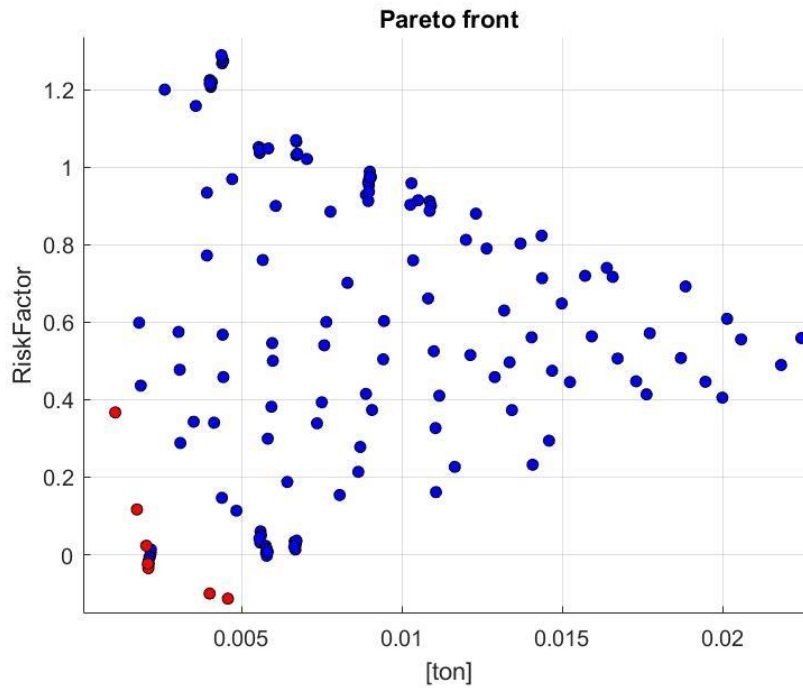


Figure 37: CASE 1 - Pareto Front

5.1.2 CASE 2 – Spur Gear

As typically rule in gears design, it is supposed that a radial and an axial and radial bearing are mounted between the shaft and gear, even if the gear is not excited in axial direction.

For this reason, one set of constrained nodes, referred to the radial and axial bearing, has only the tangential degree of freedom, while the other also has the axial one.

Moreover, the reduction of mass has been privileged over the static and dynamic performances, giving, in the weighted sum for the computation of the objective function, a weight of 1.5 to the mass and 1 to the Risk Factor.

5. Two-Parameters Optimization

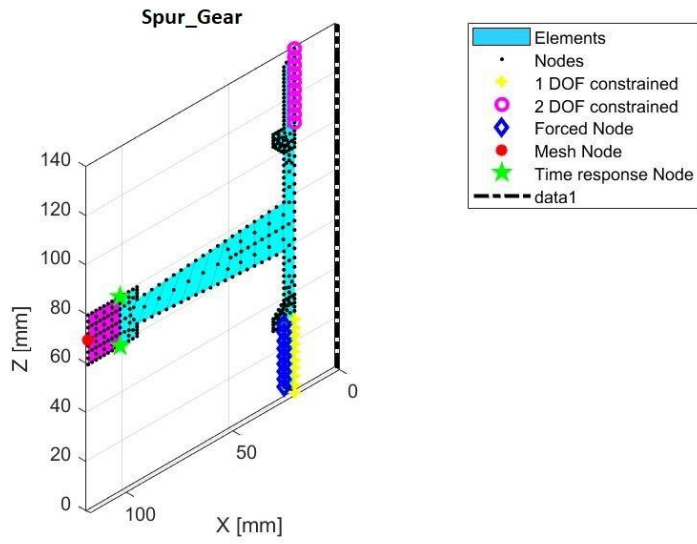


Figure 38: Case2- Forces and constrains

Also in this case, it is interesting to analyze the three-dimensional plots of the objective functions.

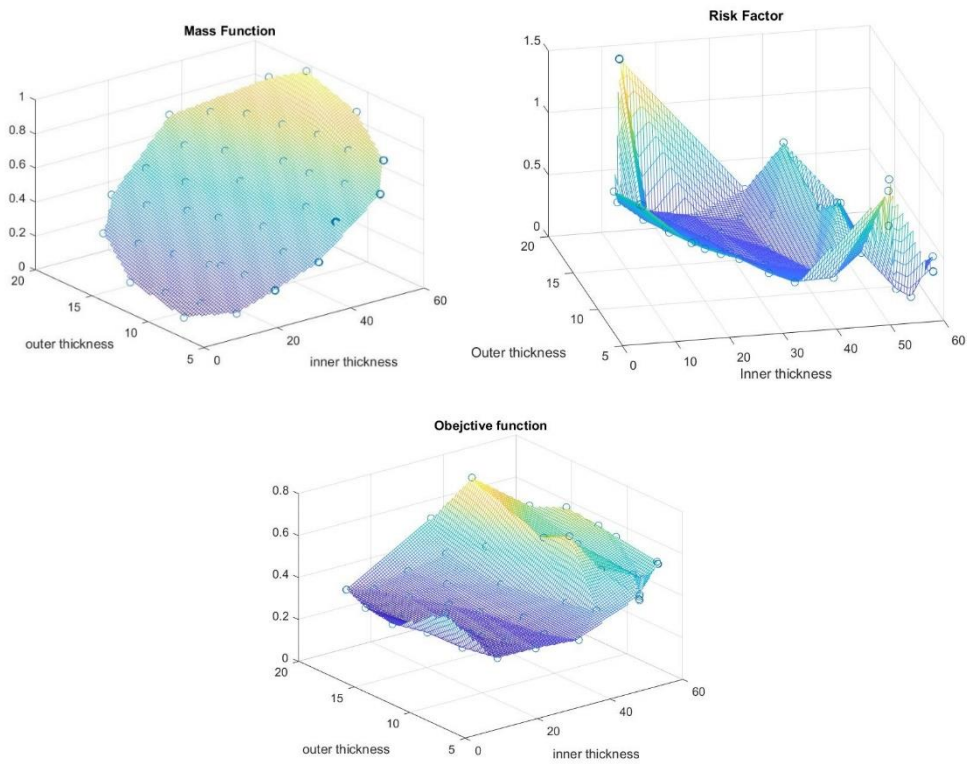


Figure 39: Case 2- Plot of Mass, Risk-Factor and Objective Functions

5. Two-Parameters Optimization

It is important to emphasize that the objective functions are smooth, since from an engineering point of view the smooth shape of a function denotes a well-defined physical problem.

The mass function has the expected trend, its values decrease with decreasing both the thicknesses. Since objective function is the weighted sum of mass and risk factor, its shape depends on the weights that the user chooses, and it can be noted that in this case it is dominated by the mass.

The risk factor is also calculated with a weighted sum and fig. 40 shows the graphs of its two terms.

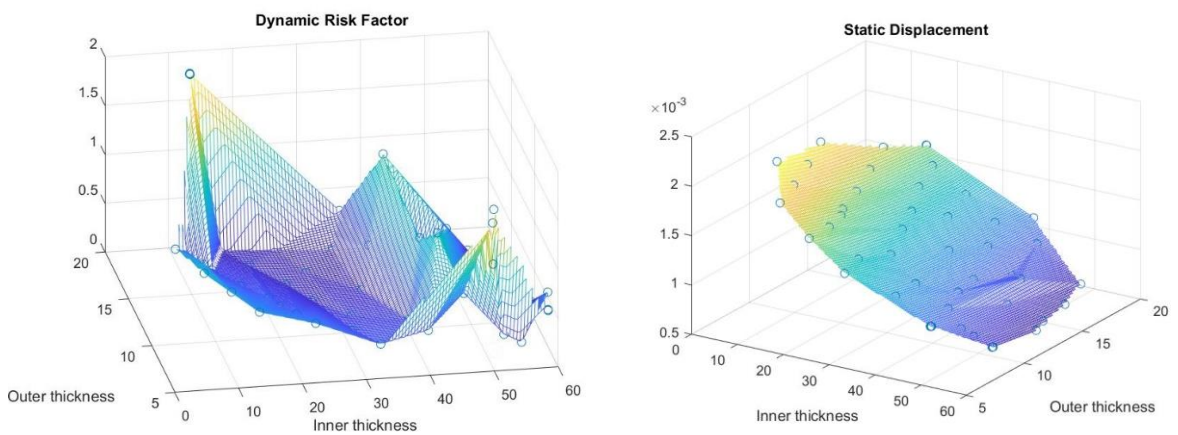


Figure 40: CASE 2- Plots of the terms of the Risk Factor function

It can be noticed that in this test the Risk factor shape is dominated by the dynamic term, since it was assigned a weight of 1 while the maximum static displacement (after normalization) was assigned a weight of 0.5.

However, each configuration that shows static displacement, both in axial end in radial direction, greater than 0.005 [m] has been discarded.

Fig. 41 shows the optimal section of the gear, that was founded in this test, while its time response is plotted in Figures 42.

5. Two-Parameters Optimization

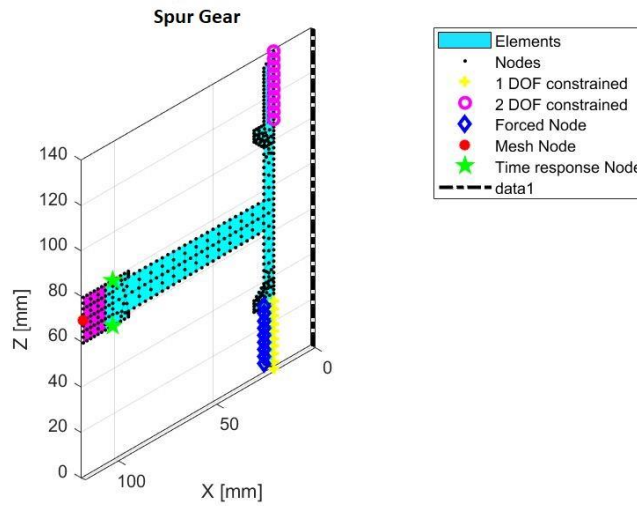


Figure 41: Case 2 - Optimal gear section

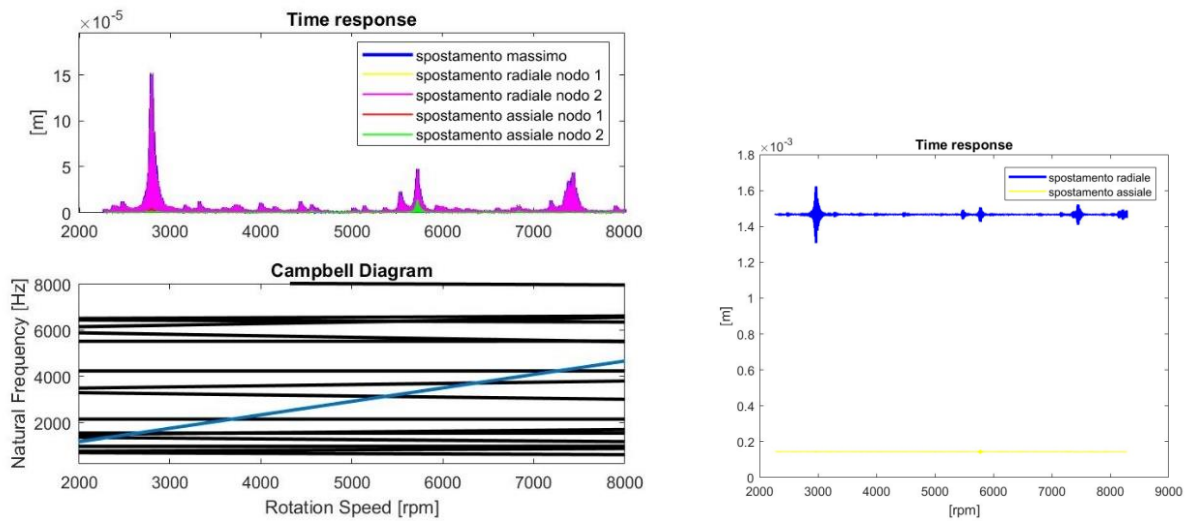


Figure 42: Campbell diagram and Time response of the optimal gear section

To understand the danger of the analyzed configuration, Fig. 43 shows the envelope of the risk function, that is related to the operative conditions, on which the amplitudes of the rescaled peaks have been overlapped.

5. Two-Parameters Optimization

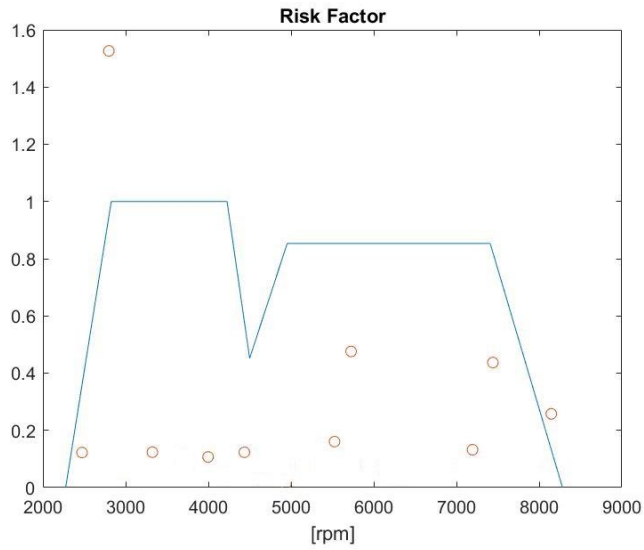


Figure 43: Optimal Section - Risk Function envelope

The time response shows only one high peak just outside the margin band, while the other peaks have smaller amplitudes.

For this reason, this parameters configuration was considered safe, how the computation of the Risk Factor confirms.

The risk related to each peak and its amplitude are listed in the table 1, to calculate the Risk Factor.

PEAK VALUE [mm]	PEAK VALUE RESCALED	PEAK POSITION [rpm]	RISK
0.012	0.12	2473	0.36
0.152	1.53	2797	0.94
0.012	0.12	3323	1
0.011	0.11	3997	0.37
0.012	0.12	4435	0.58
0.016	0.16	5526	0.85
0.048	0.48	5726	0.85
0.013	0.13	7195	0.85
0.044	0.44	7441	0.82
0.026	0.26	8147	0.13

Table 1: Amplitude, position and risk of peaks

$$\begin{aligned}
 RiskFactor_{Dynamic} &= \left(\frac{\sum_{i=1}^n PeakAmplitude_{(i)} * Risk_{(i)}}{PeaksNumber} \right)_{rescaled} = (0.095)_{rescaled} \\
 &= 0.22
 \end{aligned} \tag{5.1}$$

As it can be seen from figure 42, the maximum static displacement is in radial direction and thus, rescaling its value, it is possible to compute the Static Risk-Factor:

$$\begin{aligned}
 RiskFactor_{Static} &= \max(axial\ displacement, radial\ displacement)_{rescaled} \\
 &= (1,44 [mm])_{rescaled} = 0.69
 \end{aligned} \tag{5.2}$$

Finally, it is possible to calculate the weighted sum of the two Risk-Factors, that states how much dangerous this configuration is:

$$RiskFactor = \frac{0.5}{1.5} * RiskFactor_{Static} + \frac{1}{1.5} RiskFactor_{Dynamic} = 0.38 \tag{5.3}$$

The Pareto Front, from which the optimal parameters configuration was chosen, is represented in Fig. 44.

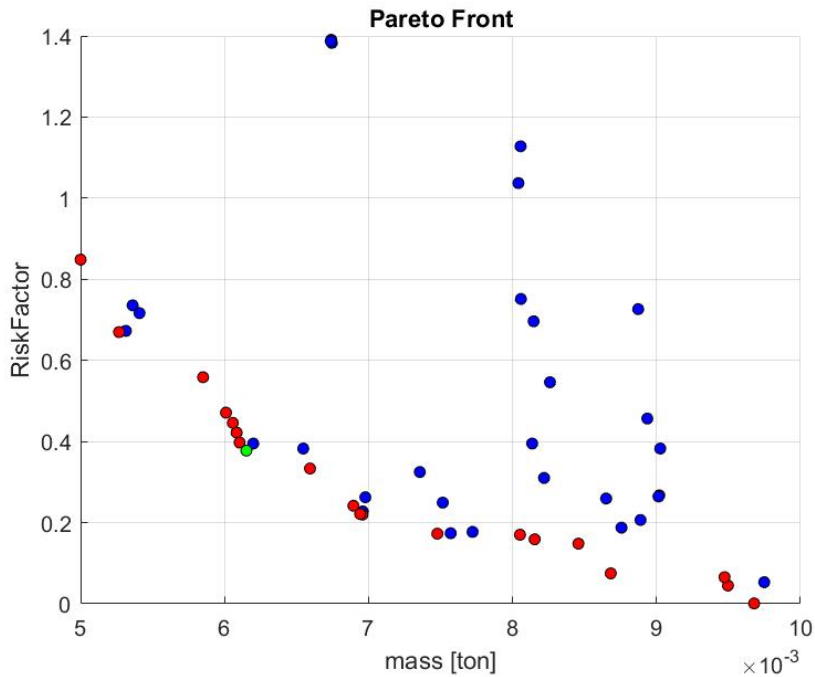


Figure 44: Pareto Front

6. Four-Parameters Optimization

In order to give more freedom to the optimization, the spur gear of the previous case, in section 5.1.2, is optimized in a four-parameter space.

As previously mentioned, the designs were optimized in two operative conditions:

OC 1: 3500 rpm – 341 N/m

OC 2: 6135 rpm – 291 N/m

and the settled objective function weights are summarized in the following table:

MASS	RISK-FACTOR _{Dynamic}	RISK-FACTOR _{Static}
1.5	1	0.5

Table 2: Objective function weights

The design space geometry was described by four parameters, that are shown in Figure 45:

- The thickness in the inner radius;
- The thickness in the outer radius;
- The axial coordinate of the midpoint in the inner radius, z_1 ;
- The axial coordinate of the midpoint in the outer radius, z_2 .

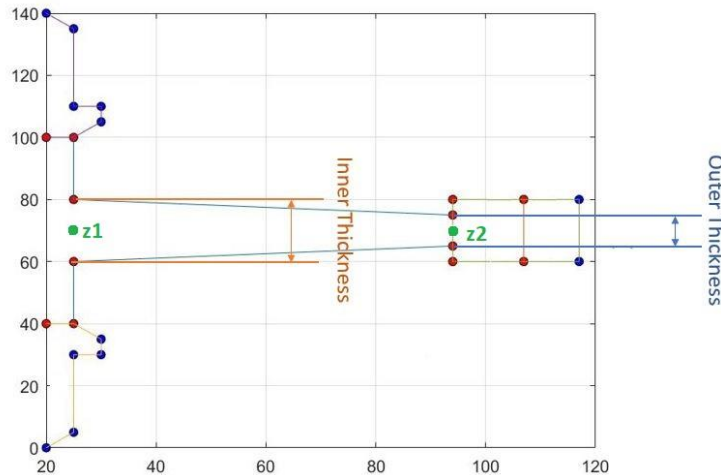


Figure 45: Representation of the optimization parameters

In this case, the formulation of the dynamic risk factor used in the previous chapter cannot be adopted, since each geometry analyzed shows a very different number of peaks in the time response from the others.

Therefore, dividing the weighted sum of the rescaled amplitudes of the peaks by the total number of peaks, the optimizer would favor a geometry that shows a time response with a high number of peaks, even if some of them are very high, compared to one that has few medium-size peaks.

For this reason, it was decided to use the following formulation of the dynamic risk factor:

$$RiskFactor_{Dynamic} = \left(\sum_{i=1}^n PeakAmplitude_{(i)} * Risk_{(i)} \right)_{rescaled} \quad (6.1)$$

6.1 Spur Gear

Fig. 46 shows the Pareto front resulting from the optimization analysis, in which the green point refers to the optimal geometry, while the optimal geometry obtained from the two-parameter optimization is marked in yellow.

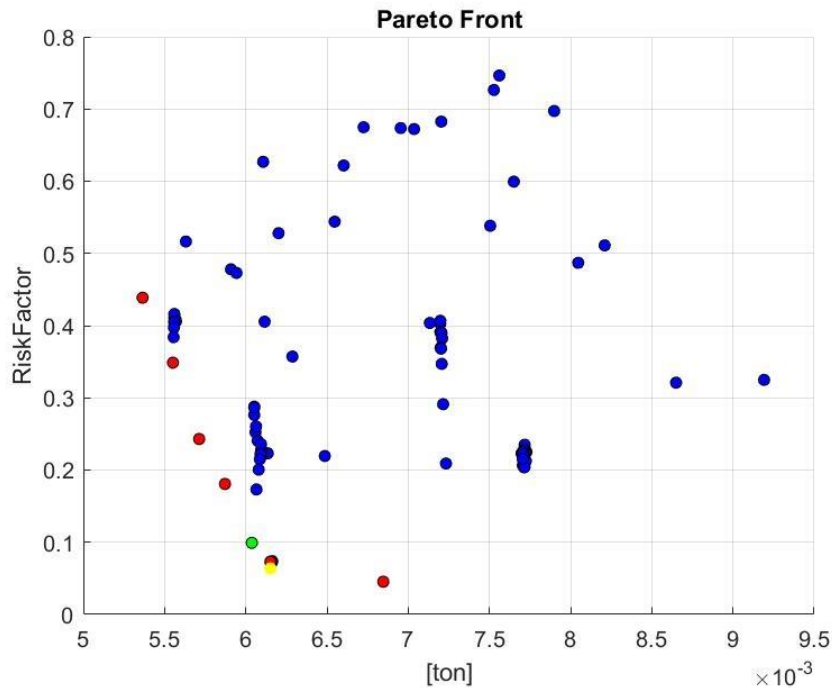


Figure 46: Pareto Front of Spur Gear Optimization

It can be noted that the optimum point of the optimization of the previous chapter still belongs to the Pareto Front, but it is not the result of the four-parameters optimization: by giving more

freedom to the optimizer, by introducing two parameters in the parameter-space, it was possible to improve the optimal geometry, reducing the mass of the gear with a little increase of its risk factor. Therefore, in a four-parameter space, it was possible to better satisfy the designer's specifications than in a two-parameter space.

In the section 6.1.1 the optimal geometry is shown and discussed, while section 6.1.2 is related to the geometry with the minimum risk factor.

6.1.1 Optimal geometry

Fig. 47 shows the geometry that was resulted from the four-parameter optimization. This is the best trade-off configuration, chosen according to the designer's specifications, expressed as an input in the weights of mass and Risk-Factor.

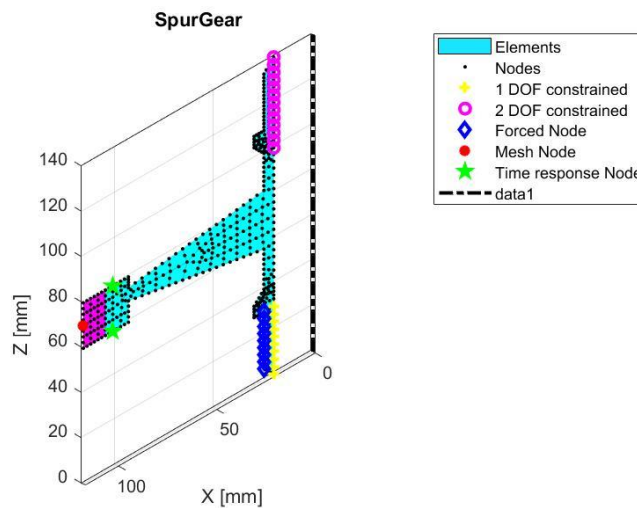


Figure 47: Optimal geometry

This configuration corresponds to a gear that weighs 6.1 kg and therefore shows a mass reduction of 1.6% compared to the result of the two-parameter optimization, at the expense of an increase in the risk factor of 55%.

Its time response and the plot of the risk envelope and of the amplitudes of the peaks, useful for calculating the Risk-Factor, are reported in figures 48 and 49.

6 - Four-Parameters Optimization

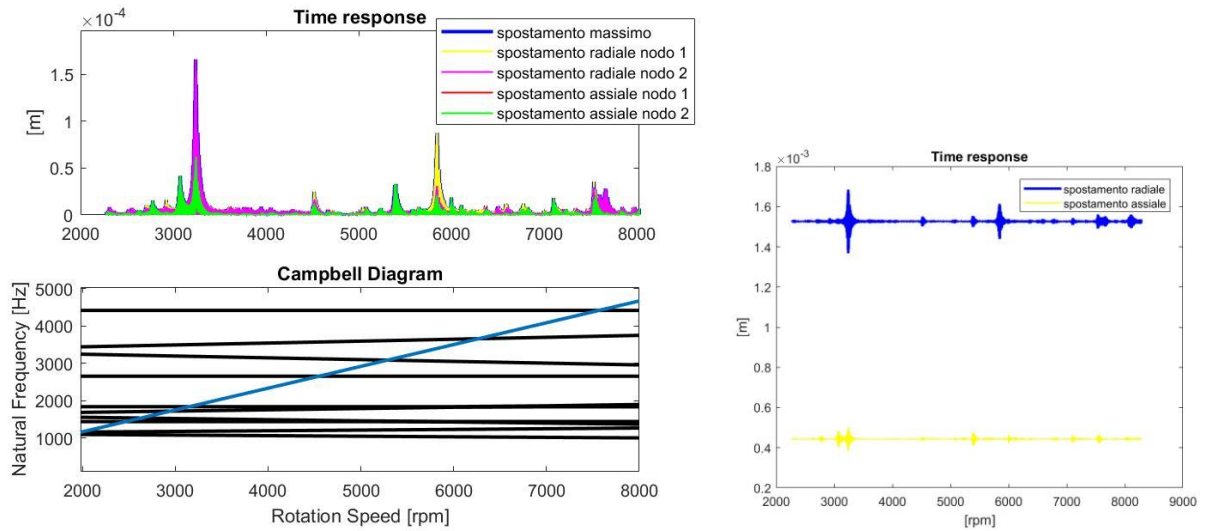


Figure 48: Campbell diagram and Time response of the optimal geometry

As it can be seen from figure 48, the maximum static displacement is in radial direction and thus, rescaling its value, it is possible to compute the Static Risk-Factor:

$$\begin{aligned}
 RiskFactor_{static} &= \max(axial\ displacement, radial\ displacement)_{rescaled} \\
 &= (1.50 [mm])_{rescaled} = 0.19
 \end{aligned}
 \tag{6.2}$$

The time response shows seven peaks, but many of which are small or out the margin band of speed, as figure 49 puts in evidence.

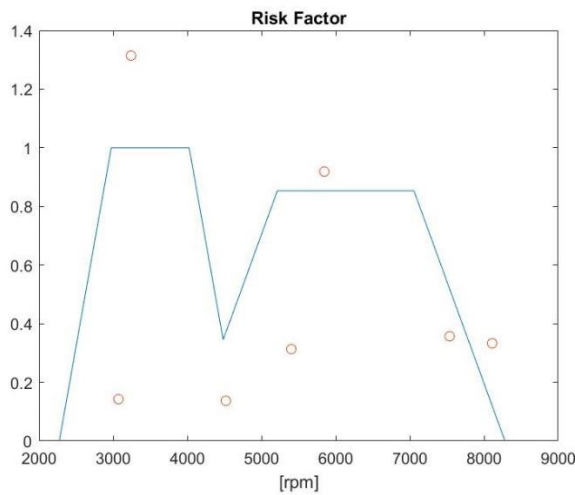


Figure 49: Risk-Function envelope of the optimal geometry

Reporting the risk related to each peak and its amplitude in the table 2, is possible to calculate the Dynamic Risk Factor:

PEAK VALUE [mm]	PEAK VALUE RESCALED	PEAK POSITION [rpm]	RISK
0.041	0.14	3078	1
0.17	1.3	3241	1
0.025	0.14	4519	0.37
0.033	0.31	5402	0.85
0.088	0.92	5847	0.85
0.035	0.36	7536	0.52
0.034	0.33	8110	0.12

Table 3: Amplitude, position and risk of peaks

$$\begin{aligned}
 RiskFactor_{Dynamic} &= \left(\sum_{i=1}^n PeakAmplitude_{(i)} * Risk_{(i)} \right)_{rescaled} \\
 &= (2.78)_{rescaled} = 0.053
 \end{aligned} \tag{6.3}$$

Finally, it is possible to calculate the total Risk-Factor, as weighted sum of the two Risk-Factors, that states how much dangerous this configuration is:

$$RiskFactor = \frac{0.5}{1.5} * RiskFactor_{Static} + \frac{1}{1.5} RiskFactor_{Dynamic} = 0.099 \tag{6.4}$$

6.1.2 Geometry with minimal Risk-Factor

The second configuration is related to the geometry with the lowest Risk-Factor and thus to the geometry with the best time response. Its section is reported in Fig. 50.

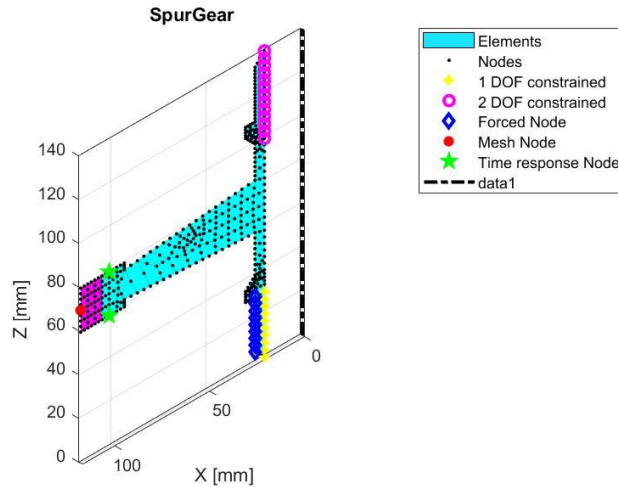


Figure 50: Geometry with minimal Risk-Factor

This configuration corresponds to a gear that weighs 6.8 kg and it shows a Risk-Factor reduction of 29 % compared to the result of the two-parameter optimization, at the expense of a mass increase of 9.7%.

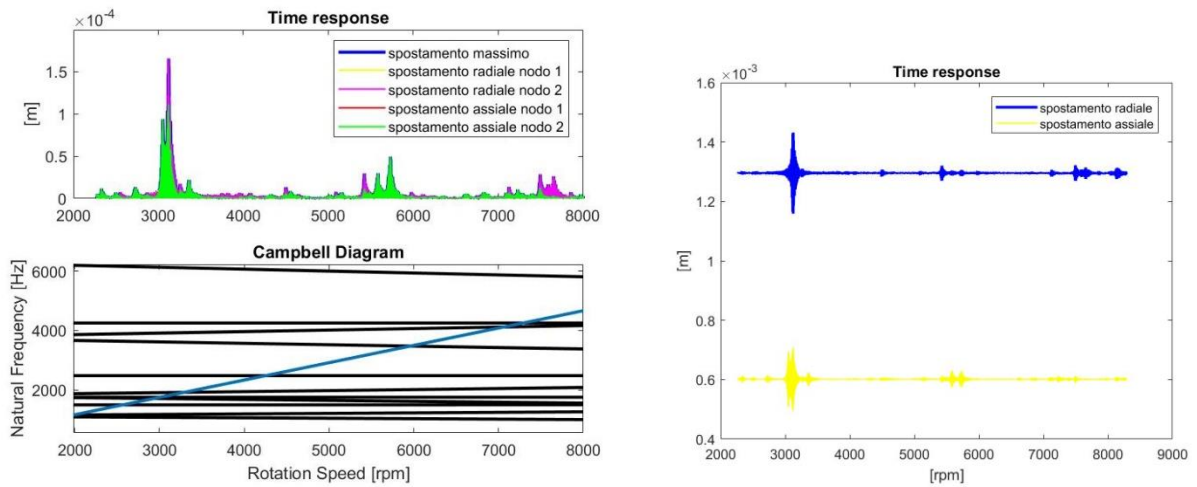


Figure 51: Campbell diagram and Time response of the geometry with minimal Risk-Factor

The maximum static displacement is in radial direction and thus, rescaling its value, it is possible to compute the Static Risk-Factor:

$$\begin{aligned}
 RiskFactor_{static} &= \max(axial\ displacement, radial\ displacement)_{rescaled} \\
 &= (1.3\ [mm])_{rescaled} = 0.136
 \end{aligned}
 \tag{6.5}$$

The time response shows seven medium-small peaks and, as previously done, reporting the risk related to each peak and its amplitude in the table 4, it is possible to calculate the Dynamic Risk Factor.

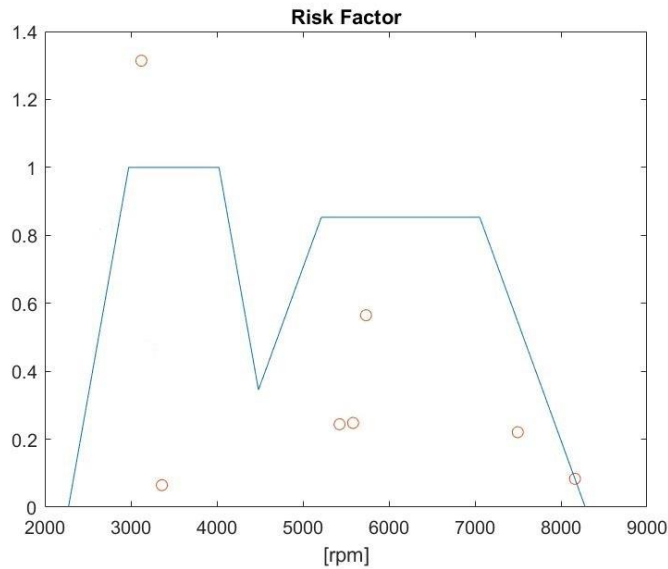


Figure 52: Risk-Function envelope of the geometry with minimal Risk-Factor

PEAK VALUE [mm]	PEAK VALUE RESCALED	PEAK POSITION [rpm]	RISK
0.166	1.31	3122	1
0.022	0.07	3361	1
0.029	0.24	5426	0.85
0.029	0.24	5587	0.85
0.050	0.56	5734	0.85
0.029	0.22	7497	0.54
0.023	0.08	8163	0.08

Table 4: Amplitude, position and risk of peaks

$$\begin{aligned}
 \mathbf{RiskFactor}_{Dynamic} &= \left(\sum_{i=1}^n \mathbf{PeakAmplitude}_{(i)} * \mathbf{Risk}_{(i)} \right)_{rescaled} \\
 &= (2.23)_{rescaled} = \mathbf{0}
 \end{aligned} \tag{6.6}$$

Therefore, the total Risk-Factor is:

$$\mathbf{RiskFactor} = \frac{0.5}{1.5} * \mathbf{RiskFactor}_{Static} + \frac{1}{1.5} \mathbf{RiskFactor}_{Dynamic} = \mathbf{0.045} \tag{6.7}$$

7. Conclusions

This thesis work starts with the aim of determine the optimal gear design.

The methodology developed belongs to the field of parametric optimization, since the cross section of the gear is parameterized and can be modeled by varying the value of the design parameters.

It is a versatile tool because it can optimize the geometry of the cross section of any axisymmetric structure and different objective functions can be settled by the designer.

Compared with topological optimization, this methodology minimizes the risk of generation of unrealistic or expensive-to-manufacture solutions, because the designer can guide the optimization process.

Another pro of this tool is that it is implemented entirely in MATLAB environment, because it permits shorter optimization process runtime than those of other tools.

However, even if the tool can guide the optimization towards statically resistant structures by minimizing the static displacements, a rigorous static analysis is needed.

Finally, a more detailed methodology used to create the cross-section geometries can be implemented, in order to consider more elaborate shapes of the design space.

Appendix A

FEM analysis

The term Finite Element Method comes from the main logic of the method itself: to solve a problem, the FEM subdivides a large system into smaller and simpler parts that are called finite elements.

This necessity born because analyzes often require solving a set of partial differential equations (PDE).

Thus, during a finite element analysis (FEA), after the domain discretization, the fundamental equations are applied to each element.

The solutions calculated on each element, which can for example be their displacements (or temperatures, stresses, etc.), are then combined in order to obtain the overall solution for the entire domain.

Because the continuous domain is discretized through a finite number of points, some evaluation errors cannot be avoided.

The aim of a good FEA is to reduce as much as possible these errors and at least to recognize it, and therefore, to obtain a solution that is as close as possible to the exact one.

Since the field of application of the tool developed in this thesis is the analysis of the behavior of gears, let's consider the formulation of a dynamic study of an elastic and inertial system:

$$\underline{\mathbf{M}}\ddot{\mathbf{q}} + \underline{\mathbf{K}}\mathbf{q} = \mathbf{f} \quad (7.1)$$

Where \mathbf{M} and \mathbf{K} are respectively the mass and the stiffness matrices, \mathbf{q} , $\dot{\mathbf{q}}$, and $\ddot{\mathbf{q}}$ are the generalized displacements, and \mathbf{f} is the external forcing term.

The previous equation can be more complex as additional factors are considered.

In general, the definition of \mathbf{M} , \mathbf{K} and \mathbf{f} can be performed through three formulations: by assigning in the element domain displacements or strains or stresses. Normally, in structural mechanical field it is used the assigning displacements formulation, in which the only variable are the displacements.

Since the cinematic description of an element through a finite number of parameters constrains the element, to perform a good FEA is important to correctly choose the shape functions by which the displacements field is approximated.

Mesh

The mesh is fully defined by a certain set of information, the so-called cell tuples: the vertices V of each element and its connectivity Q .

Formally, considering a quadrangular mesh:

$$M(V, Q) = [\{v_1, v_2, v_3, v_4\}, \{v_1, v_2\}, \{v_1, v_4\}, \{v_2, v_3\}, \{v_3, v_4\}] \quad (7.2)$$

In which the first set of vertices defines the element and the other couples of vertices define the edges of the element.

There are different types of element that can be used to discretize a domain and their correct choice depend on the studied problem.

Figure 53 shows 3 different elements that can be chosen.

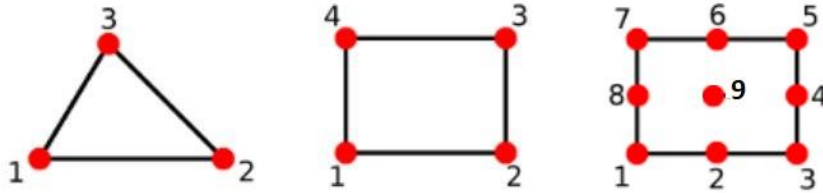


Figure 53: FEM elements

Since in the developed tool rectangular second order serendipity elements are been used, the shape functions of this element are here reported:

$$\begin{aligned} \psi_1(\xi, \eta) &= \frac{1}{4}(\xi^2 - \xi)(\eta^2 - \eta) & \psi_5(\xi, \eta) &= \frac{1}{2}(1 - \xi^2)(\eta^2 - \eta) \\ \psi_2(\xi, \eta) &= \frac{1}{4}(\xi^2 + \xi)(\eta^2 - \eta) & \psi_6(\xi, \eta) &= \frac{1}{2}(\xi^2 + \xi)(1 - \eta^2) \\ \psi_3(\xi, \eta) &= \frac{1}{4}(\xi^2 + \xi)(\eta^2 + \eta) & \psi_7(\xi, \eta) &= \frac{1}{2}(1 - \xi^2)(\eta^2 + \eta) \\ \psi_4(\xi, \eta) &= \frac{1}{4}(\xi^2 - \xi)(\eta^2 + \eta) & \psi_8(\xi, \eta) &= \frac{1}{2}(\xi^2 - \xi)(1 - \eta^2) \\ & & \psi_9(\xi, \eta) &= (1 - \xi^2)(1 - \eta^2) \end{aligned}$$

Bibliography

- [1]. Kahraman A., and Blankenship G. W., 1999, “Effect of Involute Tip Relief on Dynamic Response of Spur Gear Pairs, Journal of Mechanical Design”.
- [2]. Beghini, M., Presicce, F., and Santus, C., 2004, “A Method to define Profile Modification of Spur Gear and Minimize the Transmission Error”, AGMA Technical Paper.
- [3]. Barbieri, Scagliarini, Bonori, Bertacchi and Pellicano, “Optimization methods for spur gear dynamics”, ENOC 2008, Saint Petersburg, Russia.
- [4]. D’Alò Luca, 2017, “Multiobjective Dynamics Optimization for Aeronautical Gears”, Avio Aero-Politecnico di Torino.
- [5]. M. Casiello, 2018, “Static and Dynamic Topology Optimization for Aeronautical Gears”, Avio Aero-Politecnico di Torino.
- [6]. C. Artero, 2018, “Topology Optimization of Aeronautical Gears”, Avio Aero-Politecnico di Torino.
- [7]. E. Di Giuda, 2019, “Study of advanced parametric meshing techniques for gearbox dynamic analysis”.
- [8]. G. Genta, “Dynamics of Rotating Systems”, Springer, 2004.
- [9]. A. Gugliotta, “Elementi finiti”, Otto Editore, 2002.